HHS Public Access

Author manuscript

Nat Neurosci. Author manuscript; available in PMC 2022 May 15.

Published in final edited form as:

Nat Neurosci. 2021 December ; 24(12): 1673–1685. doi:10.1038/s41593-021-00944-z.

Multi-omic analysis of selectively vulnerable motor neuron subtypes implicates altered lipid metabolism in ALS

Hojae Lee[1,2,5,†], **Jae Jin Lee**[7], **Na Young Park**[9,10], **Sandeep Kumar Dubey**[2,3], **Taeyong Kim**[6], **Kai Ruan**[2], **Su Bin Lim**[11], **Seong-Hyun Park**[1,2], **Shinwon Ha**[1,2], **Irina Kovlyagina**[1,12], **Kyung-tai Kim**[8,13], **Seongjun Kim**[1], **Yohan Oh**[1,14], **Hyesoo Kim**[1,2], **Sung-Ung Kang**[1,2], **Mi-Ryoung Song**[8], **Thomas E. Lloyd**[2,3,4], **Nicholas J. Maragakis**[2], **Young Bin Hong**[9,10,*], **Hyungjin Eoh**[7,*], **Gabsang Lee**[1,2,3,5,*]

[1]Institute for Cell Engineering, Johns Hopkins University School of Medicine, Baltimore, MD, USA

[2]Department of Neurology, Johns Hopkins University School of Medicine, Baltimore, MD, USA

[3]The Solomon H. Snyder Department of Neuroscience, Johns Hopkins University School of Medicine, Baltimore, MD, USA

[4]Cellular and Molecular Medicine Program, School of Medicine, Johns Hopkins University, Baltimore, MD, USA

[5]The Robert Packard Center, Johns Hopkins University School of Medicine, Baltimore, MD, USA

[6]Department of Biology, San Diego state University, San Diego, CA, USA

[7]Department of Microbiology and Immunology, Kech School of Medicine, University of Southern California, Los Angeles, California, USA

[8]School of Life Sciences, Gwangju Institute of Science and Technology, Gwangju, Republic of Korea

[9]Department of Biochemistry, College of Medicine, Dong-A University, Busan, Korea

[10]Department of Translational Biomedical Sciences, Graduate School of Dong-A University, Busan 49201, Korea

[*]Corresponding author: **Dr. Gabsang Lee,** glee48@jhmi.edu, Phone: +1-443-287-8631, **Dr. Hyungjin Eoh,** heoh@usc.edu, Phone: +1-323-442-6048, **Dr. Young Bin Hong,** ybhong@dau.ac.kr, Phone: +82-51-240-2762.

Author contribution:

H.L. performed the experiments, analyzed the data and wrote the manuscript with input from all authors. J.J.L, N.Y.P, S.D., T.K., K.R., S.B.L., S.P., S. H., I. K., K.K., S.K., and Y.O. performed the experiments and/or analyzed the data. Y.O., H.K., S-U.K., M-R.S., T.E.L., N.J.M., Y.B.H., and H.E. contributed to the design, supervised the study, data analysis and interpretation. G.L. designed the study, supervised the study/experiments, data analysis and interpretation and wrote the manuscript with input from all authors.

[†]First author

Competing interests:

The authors declare no competing interests.

Code availability

The R codes used to analyze RNA-seq datasets are available from the corresponding author on reasonable request. Source data are provided with this paper.

Reporting Summary

Further information on research design is available in the Nature Research Reporting Summary linked to this article.

[11]Department of Biochemistry and Molecular Biology, Ajou University School of Medicine, Suwon, Korea

[12]Present: Institute of Physiological Chemistry, University Medical Center of the Johannes Gutenberg University Mainz, Mainz, Germany

[13]Present: Jeonbuk Branch Institute, Korea Institute of Toxicology, Jeongeup, Jeollabuk-do, Republic of Korea

[14]Present: Department of Biomedical Science, Graduate School of Biomedical Science and Engineering, Hanyang University, Seoul, Republic of Korea

Abstract

Amyotrophic lateral sclerosis (ALS) is a devastating disorder in which motor neurons degenerate, the causes of which remain unclear. In particular, the basis for selective vulnerability of spinal motor neurons (sMNs) and resistance of ocular motor neurons (oMNs) to degeneration in ALS has yet to be elucidated. Here, we applied comparative multi-omics analysis of human induced pluripotent stem cell (hiPSC)-derived sMNs and oMNs to identify shared metabolic perturbations in inherited and sporadic ALS sMNs, revealing dysregulation in lipid metabolism and its related genes. Targeted metabolomics studies confirmed such findings in sMNs of 17 ALS (*SOD1*, *C9ORF72*, *TDP43* and sporadic) hiPSC lines, identifying elevated levels of arachidonic acid (AA). Pharmacological reduction of AA levels was sufficient to reverse ALS-related phenotypes in both human sMNs and in vivo in Drosophila and $SOD1^{G93A}$ mouse models. Collectively, these findings pinpoint a catalytic step of lipid metabolism as a potential therapeutic target for ALS.

Progressive loss of spinal motor neurons (sMN) is a hallmark of amyotrophic lateral sclerosis (ALS)[1,2], which causes progressive paralysis and eventually death[3]. Around 10% of ALS cases are inherited, and over 20 genes are now known to cause familial ALS (fALS)[1]. However, 90% of ALS cases are sporadic (sALS) and caused by unknown factors[4]. Recently, human induced pluripotent stem cells (hiPSCs) have emerged as an alternative and complementary system to animal models[4,5]. One of the advantages of hiPSC systems is enabling the generation of personalized cellular models with patient-specific mutations and genetic backgrounds. Using this technique, we could develop ALS cellular models with complicated genetic modifications for fALS cases, as well as for sALS. These hiPSC-based ALS cellular models have been used to elucidate pathogenic molecular mechanisms in ALS[5–7] by comparing ALS-specific sMN and healthy sMN, although the healthy control hiPSCs have variable genetic backgrounds.

Clinical features of ALS patients show selective vulnerability depending upon the specific motor neuron subtypes. Ocular motor neurons (oMNs) are functionally intact in most patients. While motor neuron subtypes in the spinal cord, hindbrain and cortex are gradually impaired or lost during ALS progression leading to disability of voluntary movement, oMNs in the midbrain remain relatively unaffected until the final stages[8,9]. To understand the selective vulnerability, oMN have been studied as an ALS-resistant cell population[10–13]. Kaplan and colleagues compared differentially expressed genes in oMNs and sMNs of wildtype (WT) postnatal mice and found that matrix metalloproteinase-9 (MMP-9) is

a relevant gene for neurodegeneration in fast motor neurons of a *SOD1* ALS mouse model[10]. Allodi and colleagues also identified that IGF2 (Insulin-like growth factor 2) had a protective role in *SOD1* mouse model and ALS sMN *in vitro*[11]. However, it is unknown if there is any specific aberration found in human ALS sMNs common for many different mutations and sporadic cases.

One understudied hypothesis is that ALS disease might be associated with alterations in lipid metabolism[14,15]. Although previous publications have provided interesting data that allow us to speculate a relationship between ALS pathology and aberrant lipid metabolism, more systematic understanding of lipid metabolic dysregulation in ALS-specific human sMNs must be performed to elucidate the metabolic causality of altered lipid metabolism in ALS disease.

In current study, we attempted to identify cell intrinsic factor(s) that cause differential susceptibility between sMN and oMN subtypes in ALS by employing transcriptomics and metabolomics profiling. Our results reveal aberrant lipid metabolism in 17 ALS patient-derived sMN populations. One of major dysregulated metabolism pathways is the off-controlled arachidonic acid (AA) metabolism, whose pharmacological modulation unexpectedly increased the survival rates of HB9::GFP$^+$ ALS sMNs and partially reversed ALS-related phenotypes in a *Drosophila* and *SOD1^{G93A}* mouse model. These studies provide new insights into ALS pathogenic mechanism and potential therapeutic targets for both fALS and sALS.

RESULTS

PHOX2B genetic reporter system enriched hESC and iPSC-derived oMN-like molecular patterns

The transcriptional remodeling of oMN during development is different from that of sMNs in the spinal cord[16]. Initially, Nkx6.1$^+$ basal plate cells in the midbrain give rise to oMN precursors and differentiated Phox2a/b-expressing oMNs to form the ocular motor nucleus in the midbrain ventrolateral region[17–19]. We first evaluated expression of several markers for oMNs in embryonic mouse midbrains by immunohistochemistry (Fig. 1A–B’). Isl1 has been shown to be a key transcription factor in regulating oMN-specification in the developing midbrain[18], and the expression pattern of Phox2b, a homeodomain transcription factor, overlaps with that of Isl1 (Fig. 1B–B’). Previous studies using mouse genetics have demonstrated that proper expression of Phox2b is required for brachial motor neuron development, but not for somatic motor neurons including sMNs in the central nervous system (CNS)[16]. Therefore, mutations in *phox2a/b* have been shown to be specifically relevant to ocular motor genetic disorders[20]. Based on these findings, we generated PHOX2B::GFP reporter human embryonic stem cells (hESC)s and hiPSCs using the CRISPR-Cas9 system[21]. This reporter system has allowed us to develop an oMN-like cell differentiation protocol by modification of midbrain dopaminergic neuronal (mDA) differentiation methodology[22]. In the developing mouse brain, we observed that the TH$^+$ mDA neurons were located in the ventral region of midbrain, but distinctly separate from oMNs (Fig. 1A’). During neurogenesis of the ventral region of the midbrain, the sonic hedgehog (SHH) signaling pathway is one of the key regulators of oMNs specification[23].

Therefore, we modified the dosage of recombinant SHH protein/purmorphamine (PMP) treatment in the mDA differentiation method (Fig. 1C). Our new protocol significantly increased the efficiency of obtaining PHOX2B::GFP$^+$ cell differentiation compared to the mDA method (Fig. 1D–E and Extended Data Fig. 1K–L). Post-purified PHOX2B::GFP$^+$ cells showed enriched marker protein expression including ISL1, NKX6.1 and PHOX2B (Extended Data Fig. 1A–C'), suggesting that our protocol provides selective cell lineage of oMN-like hESC and hiPSC while general efficiency is low with line-to-line variations. qRT-PCR analysis also confirmed this by showing the enrichment of transcripts (*ISL1, PHOX2A*, *NKX6.1*, *EN1* and *CHAT*) expressed in oMN-like cells selected by our protocol, but not in mDA enriched cells (*NURR1*) (Extended Data Fig. 1D–I). Finally, we confirmed limited inclusion of peripheral autonomic neurons by profiling genetic expression including *EN1*, a regional marker of midbrain[21,24] and *GATA2* and *3*, specific marker for peripheral autonomic neurons[25] (Extended Data Fig. 1J).

To isolate pure oMN-like cells from ALS hiPSC lines, we also generated a PHOX2B::GFP reporter from healthy control and ALS hiPSC lines (*SOD1^{A4V}* and *C9ORF72* with 500 *GGGGCC* hexanucleotide repeats) using the CRISPR-Cas9 system (Fig. 1F–H and Extended Data Fig. 2A–C'). We found that PHOX2B::GFP$^+$ expression patterns in the hiPSC lines were similar to that of wild type hESCs (Figure 1D and Extended Data Fig. 2D–E). qRT-PCR analysis also revealed that oMN-specific marker genes (*ISL1, PHOX2A, NKX6.* and *EN1*) were enriched, but not *NURR1* transcript (mDA marker) in the post-sorted PHOX2B::GFP$^+$ cells of ALS lines as seen in PHOX2B::GFP+ cells (Extended Data Fig. 2F–K). Our qRT-PCR results also showed highly enriched neuronal maturation maker genes (*TUJ1*, *MAP2*, *CHAT* and *VACHT*) in post-sorted oMN-like cells (Supplementary Data Fig.1). Taken together, we confirmed that PHOX2B::GFP$^+$ cells-derived from healthy and ALS hESCs/hiPSCs commonly showed oMN-like profiles.

HB9::GFP$^+$ neurons represent ALS hiPSC-derived sMN cells

To compare overall transcriptomic patterns between oMN-like and sMN subtypes, we also developed a sMN-specific genetic reporter system from ALS hiPSCs. HB9 is known to be a specific transcriptional marker for sMN specification in the spinal cord[26]. Indeed, whole mount staining of *Hb9::GFP*[27] and *Isl1::GFP*[28] transgenic embryos clearly showed that projection of Isl1::GFP$^+$ cell populations was identical to Hb9::GFP$^+$ cells in the spinal cord, but not oculomotor neuronal projection in the midbrain[29](Extended Data Fig. 3A–B'). Thus, we generated an HB9::GFP genetic reporter in ALS hiPSC lines (*SOD1^{A4V}* and *C9ORF72*) using the CRISPR-Cas9 system (Extended Data Fig. 3C–D') and the stop codon in the human HB9 locus was replaced with 2A-eGFP-PGK-Puro gene cassette (Extended Data Fig. 3E). After morphological and antibiotic selection, we attempted sMN differentiation using an established sMN differentiation method as previously described[30] (Extended Data Fig. 3F–G). FACS analysis was used to confirm high numbers of HB9::GFP$^+$ cells in differentiated culture of both HB9::GFP genetic reporter ALS hiPSC lines (Fig. 1I–K). In addition, time course analysis of HB9::GFP$^+$ cells by FACS indicated that the GFP expression gradually increased beginning at D5, but then started to decrease after D13 till D17 in both ALS lines. Our qRT-PCR results using post-sorted HB9::GFP$^+$ cells (at D17) showed highly enriched mRNA expression of sMN-specific genes, including *HB9,*

ISL1, LHX3, *FOXP1,TBX20, CHAT* and *VACHT*, and significant down-regulation of pluripotent markers, *OCT4* and *NANOG* (Extended Data Fig. 3H–I and Supplementary Data Fig. 2A–H), which demonstrated that our HB9::GFP$^+$ cells are indeed enriched with sMN-specific molecular markers. To identify subtype-specific susceptibility of ALS sMN differentiation, we found comparable levels of subtype specific marker gene expression (*HB9*, *ISL1*, *MAP2*, *CHAT* and *VACHT* for sMN, *LHX3* for medial motor column, *FOXP1* for lateral motor column) at D17 and earlier time (D14) (Supplementary Data Fig. 3). FACS analysis also indicated (Fig. 1I–K and Supplementary Data Fig. 2I–J) that the majority of cells co-expressed HB9::GFP and HB9 (96.7% in *C9ORF72*, 85.3% in *SOD1^{A4V}*) as well as ISL1 and HB9::GFP (96.6% in *C9ORF72*, 88.8% in *SOD1^{A4V}*). Additionally, we found that there are increased expression levels of different *HOX* subfamily genes (*HOXA2, 5, 7* and *10*, detected by qRT-PCR) in the HB9::GFP$^+$ cells, but not in PHOX2B::GFP$^+$ cells, supporting the regional specificity of both neuronal populations (Extended Data Fig. 3I). Taken together, these data indicate that HB9::GFP$^+$ cells-derived from two different ALS hiPSC lines serve as sMN populations.

Transcriptomic differences in lipid metabolism between PHOX2B::GFP$^+$ oMN-like and HB9::GFP$^+$ sMN populations in *C9ORF72* and *SOD1^{A4V}* ALS lines were revealed by comparative transcriptome profiling

In order to identify intrinsic properties that explain selective vulnerability in sMN subtypes, we performed unbiased transcriptome analysis using post-sorted PHOX2B::GFP$^+$ oMN-like and HB9::GFP$^+$ sMN cells-derived from *C9ORF72* and *SOD1^{A4V}* ALS lines (Fig. 2A and Extended Data Fig. 5A). In time course analysis of HB9::GFP expression, the GFP signal gradually decreased after D13 (*SOD1^{A4V}*) and D17 (*C9ORF72*) of the sMN specification (Extended Data Fig. 3G). Thus, we harvested 3 different batches of differentiated PHOX2B::GFP$^+$ and HB9::GFP$^+$ cells at D17 for FACS purification.

Firstly, for further confirmation of the cellular identities of PHOX2B::GFP$^+$ oMN-like and HB9::GFP$^+$ sMNs , we compared our RNA sequencing data with a published data set[31] where transcriptomic differences between oMN and sMN were summarized based on the other published data[10,32], including oMN markers (*PHOX2A*, *PHOX2B*, *TBX20*, *EN1*, *FGF10*, *EYA1*, *EYA2*, *PLXNA4* and *SEMA6D*) and sMN markers (*HB9*, *FOXP1*, *SEMA4A*, *HOXA2*, *HOXA3*, *HOXA4*, *HOXA5*, *HOXB4*, *HOXB5*, *HOXB6*, *HOXB7*, *HOXC4* and *HOXC5*) (Extended Data Fig. 4A–C). Next, to identify common target pathways of selective vulnerability between two types of motor neurons of *SOD1^{A4V}* and *C9ORF72* lines, we focused on differentially enriched gene cohorts of the HB9::GFP$^+$ or PHOX2B::GFP$^+$ populations of *SOD1^{A4V}* and *C9ORF72* background (total 4 groups; *SOD1^{A4V}* HB9::GFP$^+$, *SOD1^{A4V}* PHOX2B::GFP$^+$, *C9ORF72* HB9::GFP$^+$, and *C9ORF72* PHOX2B::GFP$^+$ cells with 3 technical replicates) (Extended Data Fig. 5B–D). PHOX2B::GFP$^+$ and HB9::GFP$^+$ cells-derived from *SOD1^{A4V}* and *C9ORF72* lines showed clearly distinct expression patterns of enriched genes (Fig. 2B). To identify meaningful pathways that are associated with cell-type specific vulnerability, we conducted gene set enrichment analysis (GSEA) using ranked list of genes by the degree of their expression. HB9::GFP$^+$ enriched Gene Ontology (GO) terms were selected over GO terms of PHOX2B::GFP$^+$ populations, which were statistically significant in ALS

lines (Fig. 2C–D). By screening for convergent target pathways in two different ALS lines of HB9::GFP$^+$, we identified common GO terms between gene set hierarchies of each ALS mutation. Interestingly, genes involved in lipid metabolic pathways such as 'Lipid Transport (GO:0006869)', 'Lipid Localization (GO:0010876)', 'Regulation of Lipid Metabolic Process (GO:0019216)' and 'Fatty Acid Metabolic Process (GO:0006631)' were commonly enriched in both ALS lines, but the other common GOs did not show any pathway correlation (Extended Data Fig. 5E–F). To rigorously confirm whether the lipid related GO terms mentioned above can represent each cell type of ALS lines, we compared transcripts of PHOX2B::GFP$^+$ oMN-like and HB9::GFP$^+$ sMNs, regardless of the *SOD1*^{A4V} and *C9ORF72* mutations, and also compared among combined control line (hESC+hiPSC)-derived PHOX2B::GFP$^+$ oMN-like, HB9 Ab stained sMNs, and ALS hiPSC line-derived sMNs. Interestingly, we found that the significantly enriched GO terms were relevant to lipid metabolism pathways in both ALS-derived HB9::GFP$^+$ cells (Fig. 2E and I–J, and Extended Data Fig. 5G). However, we could not find such aberrant lipid metabolism in the transcriptional comparison between oMN and sMN population-derived from healthy control hESC/hiPSC lines (Fig. 2 F–H and Supplementary Data Fig. 4). We also confirmed our RNA sequencing data by qRT-PCR (with an additional 3 technical replicates) with specific primer sets for lipid metabolism related genes (*ACSM1, TMEM30B, ADAM8, PLA2G10, APOA1, GHRL, SLC27A2, CPT1A* and *LRAT*) by showing statistically enriched expression of lipid metabolism related transcripts in HB9::GFP$^+$ ALS lines (Extended Data Fig. 6A–J). Importantly, the expression patterns of identified genes were similar between the oMN-like and sMNs culture of healthy hESCs, indicating that aberrant transcriptional changes in lipid metabolism are specific to ALS pathogenesis. Taken together, these data strongly indicate that significantly altered lipid metabolism related pathways in HB9::GFP$^+$ cells of *SOD1*^{A4V} and *C9ORF72* ALS hiPSCs are a prospective target to elucidate sMN pathology in ALS.

Unbiased metabolomics analysis corroborated transcriptional discrepancies in ALS-specific PHOX2B::GFP$^+$ oMN-like and HB9::GFP$^+$ sMNs cells

To verify our RNA sequencing data and pinpoint target pathways that are involved in cell type specific phenotypic vulnerability, we set out to identify metabolic differences by performing liquid chromatography mass spectrometry (LC/MS) using post-sorted PHOX2B::GFP$^+$ cells and HB9::GFP$^+$ cells of both *SOD1*^{A4V} and *C9ORF72* ALS hiPSC lines (total 4 groups; *SOD1*^{A4V} HB9::GFP$^+$, *SOD1*^{A4V} PHOX2B::GFP$^+$, *C9ORF72* HB9::GFP$^+$, and *C9ORF72* PHOX2B::GFP$^+$ cells with 3 technical replicates) (Fig. 3A). Metabolic discrepancies between the PHOX2B::GFP$^+$ cells and HB9::GFP$^+$ cells were determined by comparing the relative abundance of ~ 3,000 metabolites selected from the Metlin database (http:://metlin.scripps.edu). Using MetaboAnalyst v.4.0, multivariate unbiased clustering analyses identified a subset of metabolites and mapped annotated pathway. The pathway mapping analysis revealed that transporters and metabolic pathways for most amino acids such as arginine, proline, glutamine, glutamate, alanine, and aspartate belonged to relatively down-regulated pathways in HB9::GFP$^+$ cells compared to those in PHOX2B::GPF$^+$ cells (Fig. 3B). Amino acid deficits with activated aerobic glycolysis were previously reported to be associated with defective energy metabolism in a murine cellular model of ALS[33], implying the reproducibility of our models. Intriguingly, the analysis showed that various lipid metabolic pathways such as sphingolipid

metabolism, glycerophospholipid metabolism and terpenoid biosynthesis as groups that belong to the most aberrantly up-regulated pathways in HB9::GFP$^+$ cells as compared to those in PHOX2B::GFP$^+$ cells (Fig. 3C). These findings are corroborated by our RNA sequencing data. A multi-omics strategy using foregoing metabolomics and transcriptomics was used to combine two different 'omics' to statistically identify functional association between them and pinpointed pathways that are perturbed among the lipid metabolic pathways of HB9::GFP$^+$ cells (Fig. 3D and Supplementary Data Table 1). Intriguingly, the Expected Score by MetaboAnalyst v.4.0[34] also supported our findings by presenting lipid metabolism related pathways including 'steroid hormone biosynthesis', 'glycerophospholipid metabolism', 'arachidonic acid metabolism' and 'fatty acid metabolism' as top-ranked pathways (Fig. 3D). Thus, extensive multi-omics analysis using metabolomics and transcriptomics results indicated that lipid-related metabolism pathways were significantly perturbed in both *SOD1*^{A4V} and *C9ORF72* HB9::GFP$^+$ cells of ALS lines and might serve as potential targets to identify new pharmacological treatments.

Activation of arachidonic acid pathway is a common metabolic signature of sMN cells with various genetic backgrounds

After our unbiased multi-omics analysis using two ALS lines, we asked whether this phenotype is common in different mutations and sporadic ALS. Thus, we set a more stringent experimental plan to analyze the 'unsorted' crude sMN culture of multiple ALS hiPSC lines (Fig. 4A and Supplementary Data Table 2). We performed a focused metabolomics analysis using ~600 selected lipid metabolite references with unsorted samples of *SOD1*^{A4V}, *C9ORF72*, *TDP43*^{Q343R} and sporadic ALS lines compared to healthy control group, (Fig. 4B–C and Supplementary Data Fig. 5A–K) (detailed cell line information described in Methods; each group had 3 independent technical replicates). This focused analysis identified highly enriched metabolites belonging to glycerophospholipid metabolism, which is corroborated by results of our RNA sequencing (Fig. 2C–E) and post-sorted untargeted metabolic analysis (Fig. 3C). Therefore, the dysregulated lipid related metabolism of sMNs-derived from four ALS hiPSC lines with various genetic backgrounds seem to be potentially common pathways in ALS pathogenesis.

To pinpoint specific pathways that are associated with ALS sMN pathology, we first classified commonly over-represented or nearly absent metabolites by statistical analysis and determined that 29 metabolites belonged to the highly represented group and 22 metabolites belonged to the downregulated group that were common in multiple ALS (*C9ORF72,* 6 lines; *SOD1*, 3 lines; , *TDP43*, 3 lines; sporadic, 5 lines; each line had 3 independent technical replicates) (Fig. 4D–E, Extended Data Fig. 7 and Supplementary Data Fig.5). We also found that the abundance of each metabolite in sMN culture of *SOD1*^{A4V} ALS hiPSC line were inversely related to that of isogenic *SOD1*^{A4V} samples (Extended Data Fig. 7C–D). Unsaturated glycerophospholipids with various chain lengths were shown to be upregulated in sMNs, while natural compounds involved in the anti-inflammatory response and antimicrobial activities were downregulated (Fig. 4B–E), implying significant risk of unbalanced redox state in sMN lines. Interestingly, one of significantly downregulated in all sMN cultures natural compound ($C_{21}H_{26}O_3$ molecular formula) was a structural analog of AA861, a known 5-lipoxygenase (5-LOX) inhibitor (Fig. 4E, Supplementary Data Fig.

5I and Extended Data Fig. 7A–B and D). 5-LOX is involved in the AA pathway that catabolizes various glycophospholipid species into downstream lipid metabolites such as AA and leukotrienes (Extended Data Fig. 10). Importantly, the levels of AA was dysregulated in plasma samples of ALS patients based on other publication[35].

Based upon our metabolomics findings, absence of AA861 analog and the previous metabolomics data of ALS patient plasma, we speculated that the loss of regulation in biosynthesis of AA may be one of the causes of lipid metabolism dysregulation common in ALS sMN, corroborated with our multi-omics analysis by indicating a significantly presented 'Arachidonic acid metabolism' with significant Expected Score (~ 9.12 by MetaboAnalyst v.4.0)(Fig. 3D). To test our hypothesis, we selected 5-LOX in AA metabolism as a target for further functional analysis, because 5-LOX activity is also known to negatively be related with AA metabolism activity in other diseases[36,37]. Taken together, our results demonstrate that altered AA metabolism serves as a prominent common metabolic phenotype in sMN culture of *SOD1*^{A4V}, *C9ORF72*, *TDP43*^{Q343R} and sporadic ALS lines.

Arachidonic acid pathway alterations cause ALS phenotypes

It is well known that the cellular level of AA is critical to cell viability and linked to disease phenotypes such as hypertension, cancer and leukemia[38,39]. To examine the functional contribution of AA metabolism to sMN pathology, we tested a set of functional analogs of AA861($C_{21}H_{26}O_3$), a known 5-LOX inhibitor[40–42], including caffeic acid (CA; 3,4-dihydroxybenenearcrylic acid), apigenin, BW755C and nordihydroguaretic acid in optimized media condition (Extended Data Fig. 8A–B). Treatment of those compounds at D11 for 12 consecutive days (until D 23, during sMN differentiation protocol, Fig. 5A) was mostly sufficient to increase the numbers of HB9::GFP$^+$ cells in *SOD1*^{A4V} and *C9ORF72* ALS lines (Fig.5B–C) (detailed information of fold change analysis is in methods). In addition, because the AA level seems to be critical for HB9::GFP$^+$ sMNs survival, we tested whether direct modulation of AA levels affects the levels of HB9::GFP$^+$ cells. The AA treatment in differentiating HB9::GFP *C9ORF72* and *SOD1*^{A4V} ALS lines decreased the percentages of HB9::GFP$^+$ cells, and increased the percentages of 7AAD$^+$ (cell death marker) cells, which were significantly reversed by CA treatment in a dose dependent manner. These data demonstrate that up-regulated AA level negatively affects viability of HB9::GFP$^+$ sMNs, and a possible direct interaction between AA and CA *in vitro* (Fig. 5D,E and Extended Data Fig. 8E–H).

To confirm the rescuing effects of CA treatment seen in our *in vitro* hESC and hiPSC sMN model, we employed a *Drosophila* model of *C9ORF72*-ALS that overexpresses 30 *G4C2* repeats[43]. Surprisingly, we observed significant dose-dependent recovery of eye degeneration phenotypes, progeny rate and survival rate in this model by CA (Caffeic acid), NDGA (Nordihydroguaretic acid) and Api. (Apigenin) (Fig. 6A–L). We next investigated whether CA could ameliorate ALS phenotype in a mouse model. We evaluated the CA efficacy with three independent experiments by administration of CA to *SOD1*^{G93A} mice from D60 to D120 of age (Extended Data Fig. 9). The first experiment (Exp 1) was for the assessment of the disease onset, survival, and behavioral test, and the other experiments

(Exp 2 and Exp 3) were for histological analyses. In the Exp 1 (n=24 for each group), we found that CA delayed the disease onset and survival. The disease onset, determined by tremor and hind-limb splay defects, was significantly delayed in CA administered group (118.8 ± 4.3 days) compared to control *SOD1*^{G93A} mice (109.8 ± 7.7 days) (Fig. 7A). The delay of disease onset was also correlated with the lifespan of the mice. The survival of *SOD1*^{G93A} mice, determined by loss of righting reflex within 30s, was also significantly extended in CA administered mice (171.0 ± 11.4 days) as compared to control mice (162.8 ± 12.3 days) (Fig. 7B). The attenuated disease symptom was also observed in locomotor performance. *SOD1*^{G93A} mice began to rapid reduction in rotarod performance from 15 weeks of age and, however, CA administration resulted in a significant slowdown of the reduction (Fig. 7C). The attenuated disease progression by CA was also observed in body weight and grip strength (Extended Data Fig. 9B–C). Next, we analyzed the integrity of motor neuron and astrogliosis using histological assessments at early symptomatic stage (16 wks, Exp 2) and late symptomatic stage (20 wks, Exp 3). The number of motor neuron (larger than 25 μm) in the ventral horn of spinal cord was significantly reduced in control *SOD1*^{G93A} mice (18.0 ± 3.5) as compared to wild-type mice (30.0 ± 2.8) at early symptomatic stage, however, the number was significantly increased by the administration of CA (22.8 ± 4.3). The significant difference was also maintained in the number of either motor neuron in the spinal cord (13.9 ± 1.8 in control vs 17.5 ± 3.8 in CA) (Fig. 7D and E) and pyramidal neuron (layer V) in motor cortex (28.5 ± 6.6 in control vs 34.5 ± 5.6 in CA) (Extended Data Fig. 9) at late symptomatic stage. Fluorescent staining with GFAP and Iba1 antibodies revealed that *SOD1*^{G93A} mice exhibited increased numbers of activated astrocytes and microglia in the spinal cord compared to wild-type mice. On the other hand, CA administration attenuated their activation (Fig. 7F–H). In addition, innervated neuromuscular junction was also significantly spared in CA treated mice and the weight of gastrocnemius muscle was correlated with the attenuated disease symptom (Extended Data Fig. 9). Collectively, these data suggested that CA-mediated pharmacological modulation of the AA pathway has a potential for therapeutic benefit for multiple ALS models.

Next, we tested how dysregulation of the AA pathway mediates ALS pathogenesis using CA treatment, an inhibitor of 5-lipoxygenase (5-LOX)[36,37], can restore the dysregulated levels of AA. We quantified the levels of AA before and after CA treatment in sMN culture of the 4 ALS lines using our focused metabolomics analysis. When comparing vehicle (ethanol) and CA (25 μg/ml) treated ALS samples (*C9ORF72,* 6 lines; *SOD1*, 3 lines; *TDP43*, 3 lines; sporadic, 5 lines) sMN culture), we observed significantly decreased levels of AA in CA-treated ALS samples (Extended Data Fig.10A–F). Collectively, CA treatment reverses ALS-related phenotypes through the metabolic modulation of AA, suggesting that AA metabolism might be a rich source of promising drug targets for multiple ALS cases, and CA serves as a chemical scaffold of AA inhibitors (Extended Data Fig.10G).

DISCUSSION

Here, through unbiased comparative multi-omics analyses of two distinct motor neuron subtypes (oMN-like PHOX2B::GFP$^+$ and HB9::GFP$^+$ sMNs), we identified that various pathways in lipid metabolism, especially the AA metabolic pathway, are dysregulated in *SOD1*^{A4V} and mutant *C9ORF72* HB9::GFP$^+$ populations but normal in PHOX2B::GFP$^+$

populations. These findings were also validated by a targeted metabolomics study between healthy and 17 ALS lines neuronal populations. Importantly, we were able to rescue the ALS phenotypes, both *in vitro* and *in vivo,* by chemical regulation of the AA metabolism, showing an untapped translational potential of findings described in this study.

Previously, several groups have suggested therapeutic target molecules[10,44,45], but our transcriptome analysis results did not confirm those findings (Supplementary Data Fig. 4D). One possible reason is species and/or mutation differences between the *SOD1*^{G93A} mouse strain and our *SOD1*^{A4V} hiPSC-derived sMNs. For example, one previous study identified *MMP-9* gene in a comparison of oMNs and sMNs in WT mice[10], but our comparative analysis was conducted on ALS-specific human oMN-like and sMNs in *SOD1*^{A4V} and *C9ORF72* mutations. Our comparative analysis between human oMN-like PHOX2B::GFP^{+} and HB9::GFP^{+} sMNs revealed significant changes in lipid metabolism pathways in ALS sMN populations. Interestingly, the expression levels of DEGs within the lipid metabolism pathways were mostly comparable in healthy oMN-like and sMNs, although transcriptomic profiling of healthy control hiPSC-derived different motor neurons is difficult to interpret the comparison between genetic reporter and antibody staining based approach, suggesting that the aberrant transcriptional levels in lipid related pathways is unique to the ALS background (Supplementary Data Fig. 4). Furthermore, we attempted to pinpoint specific pathways using our transcript profile by incorporating metabolomics analysis and assembling puzzle pieces. We independently conducted targeted metabolomics of four ALS (*SOD1*^{A4V}, *C9ORF72, TDP43*^{Q343R} mutations and sporadic hiPSC lines)-derived sMN differentiation to confirm the unbiased multi-omics results. As a result, we confirmed significant numbers of highly enriched (29 metabolites) or downregulated metabolites (22 metabolites) common in four ALS (*C9ORF72,* 6 lines; *SOD1*, 3 lines; *TDP43*, 3 lines; sporadic, 5 lines) hiPSC-derived sMN cultures. Interestingly, the results of metabolomics and multi-omics not only consistently showed lipid metabolism, but also the pentose phosphate pathway (PPP) as well as histidine metabolism (Fig. 3C and D and Fig. 4D) and purine/pyrimidine metabolism (Fig. 3D and 4B) are dysregulated. Aberration of PPP together with nucleotide metabolism might be a metabolic signature of higher burden of DNA damage due to higher ROS level and redox imbalance[46,47] in ALS sMN compared to healthy-derived sMN or ALS-derived oMN, which is corroborated by previous ALS studies[9,48,49]. Taken together, our data clearly show that there is aberrant lipid homeostasis in sMN cultures of ALS hiPSCs and also imply that dysregulated lipid metabolic pathways might serve as therapeutic target for ALS patients.

Consistent with our findings, accumulating evidence has also shown potential connections between ALS pathogenesis and aberrant lipid mechanisms[14,15,44,50–53], but there are few proven detailed mechanistic studies. To the best of our knowledge, the present study is the first report providing systematic comparison between ‘clinically affected’ HB9::GFP^{+} sMN versus ‘clinically non-affected’ PHOX2B::GFP^{+} oMN-like cells-derived from human ALS *SOD1*^{A4V} and *C9ORF72* hiPSCs, revealing the causative contribution of lipid metabolism dysregulation to ALS pathogenesis by employing RNA sequencing and metabolomics analysis. These data were also consistent with another set of analysis for targeted metabolomics between healthy donor and 17 ALS (Supplementary Data Table 2) patient-derived sMN culture. Based on the multi-omics data analysis, one of the aberrantly

regulated lipid metabolism pathways in ALS-derived sMN populations is the AA pathway. We also identified that $C_{21}H_{26}O_3$, an AA861 structural analog, is almost undetectable in sMN of ALS hiPSC lines (*SOD1*^{A4V}, *C9ORF72, TDP43*^{Q343R} and sporadic) by metabolomics analysis. Indeed, AA861 is a well-known natural inhibitor of 5-lipoxygenase (5-LOX) that metabolizes AA into other metabolites, which is consistent with the multi-omics data. Interestingly, AA levels are closely associated with apoptosis, suggesting that metabolic pathways regulating AA levels might be a therapeutic target for ALS[38,41,54]. For example, another group showed that AA modulation by PLA2 (phospholipase A2) inhibitor has a protective effect in SOD1 mouse model[55]. Therefore, we hypothesized that pharmacological modulation of the AA pathway could restore the levels of AA as well as ALS-relevant phenotypes. Indeed, treatment of several 5-LOX inhibitors was sufficient to restore the decreased levels of ALS-derived HB9::GFP$^+$ cells (Fig. 5B–C), eye degeneration phenotypes and survival rates in the *Drosophila* model (Fig. 6A–L) and *SOD1*^{G93A} mouse (Fig. 7). Considering the fact that CA treatment significantly decreased levels of AA in confirmatory metabolomics analysis (Extended Data Fig. 10A–F) and AA-induced cell death was rescued by CA treatment in a dose-dependent manner in our ALS sMN cultures (Fig. 5D–E), it is clear that inhibition of 5-LOX activity can tune down the levels of AA in ALS-derived sMN culture. However, at this moment, it is not clear how the lower levels of AA is linked to the increased levels of phospholipid species, which might be explained by Lands cycle[37,56].

Previously, another group reported that increased levels of ceramide were identified in the CSF of ALS patients, and pharmacological inhibition of the sphingolipid synthesis pathway by ISP-1 could inhibit spinal motor neuron death *in vitro*[14]. To find relevance of other lipid pathways in our study, we tested two additional candidate metabolites that are not detected in the four ALS line -derived sMNs (Ajamaline and Creatine) and two chemical compounds that can compensate for altered levels of metabolites (R-Deprenyl hydrochloride and ISP-1 for decreasing the dys-regulated levels of Putrescine and Ceramide (d18:1/16:0), respectively) (Supplementary Data Fig. 5 and Extended Data Fig. 8C–D). Furthermore, several studies by MS analysis also demonstrated that they identified phosphatidylcholine (36:4)[57] and cholesteryl esters[58]. However, we could not see any phenotypic rescuing effects in the ALS-derived HB9::GFP$^+$ sMN survival assay (Extended Data Fig. 8C–D). These data indicate that the AA pathway might play a pivotal role in ALS disease progression, at least in hiPSC-derived sMNs. In addition, another study focused on TNFα alteration in microglia cells and neuroinflammation showed pharmacological modulation of the AA pathway (by nordihydroguaiaretic acid), and improved survival rate of *SOD1*^{G93A} mouse[59]. Our data, however, cannot exclude a possible role of non-cell autonomous mechanism of the AA effects. Collectively, our studies provide extensive targeted metabolomics profiles of ALS sMN culture and identified the commonly present or undetectable metabolites as potential therapeutic targets, as shown in the example with AA861/CA.

Taken together, our data demonstrate that substantially dysregulated lipid metabolism pathways are common in 17 different ALS hiPSC-derived sMN cultures, and pharmacological modulation of AA metabolism shows protective effects in an *in vitro* human sMN model and a *Drosophila* and *SOD1*^{G93A} mouse model. Current study provides a new framework for disease modeling by comparing affected and non-affected cell types

from a disease hiPSC line, leading to the unraveling of metabolic aberrations in ALS sMN and identification of potential drug candidates. However, it remains to identify how the different genetic and sporadic ALS hiPSC lines present a converged phenotype, aberrant AA pathway, and how the 5-LOX inhibitors can rescue the phenotypes in future study.

METHODS

Generation of reporter lines in hESC/iPSC by CRISPR-Cas9

CRISPR-Cas9 knock-in strategy was performed as previously described[60]. Feeder-free H9 hESCs, 01582 hiPSCs (PHOX2B::GFP)[21], and *C9ORF72* and *SOD1*^{A4V} iPSC lines (PHOX2B::GFP and HB9::GFP) were dissociated using Accutase (Innovative Cell Technologies Inc.). Cells (2×10^6) were resuspended in nucleofection solution V (Lonza) with 4 μg of hCas9 - gRNA plasmid (gRNA #1 and #2 were used for HB9::GFP) and 4 μg of dsDNA donor plasmid. The nucleofection was performed by Nucleofector™ II according to manufacturer's instruction (B-16, Lonza), then nucleofected cells were plated on puromycin resistant MEFs (DR4, Global Stem) in hES medium (DMEM/F12 (Invitrogen) containing 20% knockout serum replacement (KSR, Gibco), 0.1 mM MEM-NEAA (Gibco), 1 mM L-glutamine (Gibco), 55μM β-mercaptoethanol (Gibco), 4 ng/ml FGF2 (Gibco)) with 10 μM Y-27632 (Cayman Chemical). After 3 or 4 days, knock-in cells were selected by treatment with 0.5 μg/ml puromycin (MilliporeSigma) in hES medium. After selection, puromycin resistant colonies were verified for GFP expression by FACS analysis using each differentiation protocol.

Plasmid constructions

For the PHOX2B::GFP reporter line, plasmids were used as previously described[21]. For the HB9::GFP reporter line, left arm 1512bp and right arm 900bp were designed from stop codon of the human *HB9* locus. Each arm was generated by PCR using (H9) hESC genomic DNA and inserted into OCT4-2A-eGFP-PGK-Puro donor vector backbone (Addgene #31938)[61] between BamHI and NheI for left arm and AscI and NotI for right arm. The gRNA sequence was designed by Zhang lab gRNA design resource[60] and subcloned into gRNA vector (Addgene #48138) as previously described[62]. All insert sequences were verified by DNA sequencing (JHU synthesis & sequencing facility).

HB9	left arm	F: ATAGGATCCTCAACTCCTGGGCTTCCCGGAACCT
		R: ATAGCTAGCCTGGGGCGCGGGCTGGTGGCTGGGC
	right arm	F: ATAGGCGCGCCGAGCCCCGCGCCCAGCAGGTGCGGC
		R: ATAGCGGCCGCCCCGGGACAGGTGTGCACCAGGCAG
	gRNA#1	F: CACCGTACAGCAACGGCGCCAGCGT
		R: AAACACGCTGGCGCCGTTGCTGTAC
	gRNA#2	F: CACCGCGGAGGACGACTCGCCGCCC
		R: AAACGGGCGGCGAGTCGTCCTCCGC

hESC/iPSC culture and differentiation

H9 hESCs, 01582 (GM01582) iPSCs (derived from each fibroblasts, Coriell Institute) and OCT4::GFP in hESC (H9), PHOX2B::GFP in hESC (H9) and 01582 iPSC, *C9ORF72*, $SOD1^{A4V}$ for PHOX2B::GFP and HB9::GFP (ALS patient fibroblasts (JH078[*C9ORF72*][63] and GO013 [$SOD1^{A4V}$][64] were collected at Johns Hopkins hospital with patient consent)[65]. $TDP43Q^{343R}$, sporadic ALS and isogenic control of $SOD1^{A4V}$ (gift from Kevin Eggan) iPSC (detailed line information in Supplementary Data Table 2)[5,6,64–68] were cultured (passages 12–60) on inactivated mouse embryonic fibroblasts (MEF, Applied Stem Cell) with hES medium at 37 °C and 5% CO_2 in a humidified incubator as described previously (Supplementary Data Table 2)[69]. For neuronal differentiation, LSB (LDN193189 + SB431542) protocol was used as described previously[70,71] and adapted for each neuronal differentiation.

FACS analysis and sorting

Cells were dissociated using Accutase after incubation for 20 min at 37 ℃ and suspended with buffer containing 40 μg/ml DNase Ⅰ (Roche Applied Science). For GFP analysis, BD FACS Calibur (Becton Dickinson) and FlowJo software (Tree Star Inc.) were used. To purify GFP^+ populations for each reporter line, a MoFlo high-speed sorter (Dako Cytomation) in the Johns Hopkins School of Public Health Flow Cytometry Core Facility and a BD FACSJazz sorter in the Stem Cell Core Facility of Johns Hopkins Medicine (Institute for Cell Engineering) were used.

Immunofluorescence staining

For Immunohistochemistry, E12.5 midbrain was dissected and fixed with 4% paraformaldehyde (PFA) overnight. After fixation, tissues were washed with PBS and incubated with 30% sucrose for cryosection as described previously[72]. The following antibodies were used as a primary antibody: rabbit anti-TH (Pel-Freez Biologicals, P40101, 1:1000), mouse anti-Isl1 (DSHB, 40.2D6, 1:100) and rabbit anti-Phox2b (gift from Jean-Francois Brunet, 1:1000)[73]. For Isl1 staining, a mouse on mouse kit (Vector Laboratory) was used. For immunocytochemistry, cells were fixed with 4% PFA and stained with mouse anti-ISL1 (DSHB, 40.2D6, 1:100), mouse anti-NKX6.1 (DSHB, F55A10, 1:100), rabbit anti-TUJ1 (BioLegend, PRB-435P, 1:1000), mouse anti-TUJ1 (BioLegend, MMS-435P, 1:1000) and rabbit anti-PHOX2B (gift from Jean-Francois Brunet, 1:1000). For FACS analysis, cells were fixed with 4% PFA and stained with mouse anti-HB9 (DSHB/concentrated, 81.5C10, 1:100) and mouse anti-ISL1 (DSHB, 40.2D6, 1:100) as described previously[74]. For 7AAD analysis by FACS, staining was conducted based on commercial instruction (BD #559925). Appropriate Alexa Fluor 488, 568 and 647 (Life Technologies (Thermo Fisher), A-11034, A-11031, A-11001, A-11036, A-21245, A-21236 ,1:1000) labeled secondary antibodies were used with DAPI (Roche Applied Science) for nuclear staining. All images were visualized with fluorescence microscopy (Eclipse TE2000-E, Nikon).

qRT-PCR analysis and primer information

Total RNA was extracted using TRIzol Reagent (Life Technologies) and reverse transcribed using High Capacity cDNA Reverse Transcription kit (Applied Biosystem). qRT-PCR was

performed using SYBR Green PCR Master Mix (Applied Biosystems) and Mastercycler ep Realplex2 (Eppendorf) with the primers shown below. Data was normalized by GAPDH expression level and all primers were designed using GenScript primer design software.

Gene	Forward	Reverse
GAPDH	TGCACCACCAACTGCTTAGC	GGCATGGACTGTGGTCATGAG
OCT4	AGTGAGAGGCAACCTGGAGA	ACACTCGGACCACATCCTTC
NANOG	CATGAGTGTGGATCCAGCTT	CCTGAATAAGCAGATCCATG
ISL1	GGTTTCTCCGGATTTGGAAT	CACGAAGTCGTTCTTGCTGA
EN1	TCTCGCTGTCTCTCCCTCTC	CGTGGCTTACTCCCCATTTA
TBX20	GGGAGGATGGTCACCTGAAA	CTGGCTGTGATGTCAGCTTC
PHOX2A	CCGATGGACTACTCCTACCTCA	GCAGGGGGCTGTATTGGAAG
PHOX2B	CCAGTGCCAGCCCAATAGAC	TGGACAATAGCAAAGCGGTTG
GATA2	CGGTCCTGCACAGATTCCCA	CAGCAGCTTCGGCCTCAAAG
GATA3	CGGAGGAGGTGGATGTGCTT	GCCCTGACCGAGTTTCCGTA
NURR1	CAAGTCACATGGGCAGAGATAG	GGCTAGGAGGGTTACAGAAATG
HOXA2	ACAAGTACCTTTGCAGACCC	CATTTCCCTTCGCTGTTTTGG
HOXB2	TTTAGCCGTTCGCTTAGAGG	CGGATAGCTGGAGACAGGAG
HOXA5	GGCCTTCCGTCCCTGAGTAT	GCAACGAGAACAGGGCTTCT
HOXA7	TCTCCCTCCTCTGTCACCCT	CCCGACCCTCTGTCCTCATT
HOXA10	GCCTGAGGTCAATGGTGCAA	AAAGTCAAGCCCGTTTGCCA
HB9	GCACCAGTTCAAGCTCAAC	GCTGCGTTTCCATTTCATCC
FOXP1	AGACAAAAAGTAACGGTTCAGCC	CGCACTCTAGTAAGTGGTTGC
LHX3	GCTGGGCCCGGGAAAGTTCG	GTGCTAGCAGCAGGTCGCCTC
NKX6.1	GAGATGAAGACCCCGCTGTA	GACGACGACGAGGACGAG
MAP2	CAGGAGACAGAGATGAGAATTCC	CAGGAGTGATGGCAGTAGAC
CHAT	GACGTCTGACGGGAGGAG	TCAATCATGTCCAGCGAGTC
VACHT	GGCATAGCCCTAGTCGACAC	CGTAGGCCACCGAATAGGAG
ACSM1	AGGAGGGCAAGAGAGGTCCA	ACCAGCCACCACTCAGGAAC
PSAPL1	CACTCATCCGCCACCAAAGC	CCTTGCTCCTCCTGCCTCTC
SYNJ2	GACAGACAGGGTGCTGTGGT	TTGTAGCTCCGCACGACCAT
TMEM30B	ATCCGCCAGGGCAACTACTC	CCACCCATCCACGAGATGCT
ADAM8	CCCACCCTTCCCAGTTCCTG	GGTGCGAACGTTGGCTTGAT
ABCG1	GCTTCCTCAGTCCAGTCGCT	CATGCTCGGACTCTCTGCCA
PPARA	CAGAACAAGGAGGCGGAGGT	GTTTGCGAAGCCTGGGATGG
SLC27A6	CGCGCCACACTTCTCTAGGT	ACGAAACACGGTGGGAGTGT
SLC27A2	CGTGGCGCTCCTTATGGGTA	CACTGGAAGCAGTGCAGCAG
PPARG	TGGTCTTGTCGGCAGGAGAC	CCCAAAGTTGGTGGGCCAGA
LRAT	CCTGGCCTGCAGGATGAAGA	CCTCGGTGGAAAGAGCTGGT
PLA2G10	TGTGTGCCTGCCAATCATGC	ACAACCCACAGTTCCTGCCA
APOA1	AAGGCCACCGAGCATCTGAG	ATTCTGAGCACCGGGAAGGG
GHRL	GCATGCTCTGGCTGGACTTG	GCTTGGCTGGTGGCTTCTTC
CPT1A	GTCACCATGCGCTACTCCCT	GCAGCGATGTCTGGAAGCTG

Gene	Forward	Reverse
SOAT2	CCTAGGCCCTGGGATGTGTG	GAAGGGCTCTCGGCTCATGT
CASPASE3	TATTCAGGCCTGCCGTGGTA	GGCACAAAGCGACTGGATGA

Motor neuron compound screening and analysis

sMN differentiation was performed as previously described[30]. For general sMN culture media, neurobasal medium (Gibco) containing B27 (Gibco), N2 (Gibco), and 2 mM L-glutamine was used as a normal medium. For compound testing, neurobasal medium with N2 was used as a conditioned medium using caffeic acid (Sigma, C0625), R-Deprenyl hydrochloride (Sigma, M003), Ajamaline (MP Biomedicals, 4360-12-7), Creatine (Sigma, 1150320) and ISP-1 (Sigma, M1177), BW755C (Tocris, 105910), Nordihydroguaiaretic acid (Sigma, 74540), Apigenin (Fisher Scientific, 50908414). For Arachidonic acid testing, Arachidonic acid (Cayman, 506-32-1) was treated in normal media. For mitomycin C treatment, 1 μg/ml of mitomycin C was treated in differentiating oMN or sMN cells for 1 hr. at D17 and analyzed after 2 days (D19) by FACS. For fold change value, non-treated % of GFP^+ were considered as a control and fold change values were normalized upon % of GFP expression of non-treated cells by FACS.

RNA sequencing

Total RNA was extracted using miRNeasy mini kit (Qiagen) as per manufacturer's instructions. RNA concentration and purity were assessed by Nanodrop (Thermo Fisher), and RNA integrity was assessed using the Agilent Bioanalyzer. cDNA Libraries were prepared for mRNA-enriched sequencing using TruSeq Stranded mRNA kit (Illumina). This was followed by normalization to 6 nM and pooling of libraries, followed by single end 75 bp sequencing on the Illumina HighSeq 4000. RNA-sequencing reads were aligned to the human reference genome (gencode.v27.primary_assembly.annotation.gtf downloaded from Gencode) using STAR aligner[75]. Differential gene expression analysis was performed using EdgeR (v3.28.0)[76] and Limma-Voom (v3.42.0)[77]. The Limma-Voom package was used for data normalization and generation of differential expression gene matrices. Genes with |fold change (FC)| >= 2 and adjusted p-value < 0.05 were considered as differentially expressed genes; 4,016 up-regulated and 3,749 down-regulated DEGs were identified. To reduce the number of differentially expressed genes, the Treat method[78] was used to calculate p-values from empirical Bayes moderated t-statistics with minimum log-FC requirement. The number of differentially expressed genes was reduced to a total of 1,806 DEGs for comparison of HB9::GFP^+ versus PHOX2B::GFP^+. To identify enriched transcriptomic signatures out of the large number of DEGs between HB9::GFP^+ and PHOX2B::GFP^+, we used a non-parametric method, gene set enrichment analysis (GSEA), where the enrichment score reflects the degree to which a gene set is over-represented at the top or bottom of a ranked list of genes[79]. Enrichment analysis and visualization were performed using clusterProfiler R package (v3.1.4.3)[80] and biological process terms from Gene Ontology (GO) with gene set size between 15 and 300 genes (GEO dataset id: GSE132972). To validate our oMN-like and sMN populations, our datasets were compared with previous mouse dataset from a previous literature where transcriptomic signature of oMN and sMN was well established[31]

(GEO dataset id: GSE118620). The mouse dataset was aligned to mouse reference genome (gencode.vM24.primary_assembly.annotation.gtf downloaded from Gencode) and further analyzed in the same way as our human dataset is analyzed. For healthy control of hESC and hiPSC lines, post-sorted oMN-like cells were differentiated from hESC/hiPSC PHOX2B::GFP lines, and sMN cells from hESC/hiPSC lines were stained by HB9 antibody (DSHB/concentrated, 1:100). A pooled library of 12 samples was subjected to Illumina platform (NovaSeq6000 S4) in 150 bp paired-end mode. Raw data (FASTQ files) were imported into Altanalyze v2.1.4 software, which uses the embedded software Kallisto and Ensembl 72 annotations. Two QC-failed control samples were excluded from the analyses. Processed expression files, including transcript-level expression values (TPMs) summed at the gene-level and read counts, were used in R (v4.0.3) to generate volcano plot, principal component (PC) plot, heatmaps, and dot plots shown in Figure 2 and Supplementary Data Figure 4. The voom function in the limma package (v3.46.0) was used to identify genes having |fold change (log2-base)|>2 and adjusted p-value<0.05, which were considered differentially expressed (DE). The prcomp function in the stats package (v4.0.3) was used to perform PC analysis using DE genes in ALS sMN samples (HB9::GFP$^+$ cells of *C9ORF72* and *SOD1*^{A4V}). The pheatmap function in the pheatmap package (v1.0.12) was used to generate heatmaps which clustered rows and columns (Pearson correlations). The enrichr fuction in the enrichR package (v3.0) was used to perform enrichment analysis of up-regulated gene sets using GO Biological Process (2018) database (GEO dataset id: GSE173115).

LC-MS metabolomics

Liquid chromatography mass spectrometry (LC-MS) differentiation and detection of each metabolite (*C9ORF72* PHOX2B::GFP$^+$, *SOD1*^{A4V} PHOX2B::GFP$^+$, *C9ORF72* HB9::GFP$^+$, *SOD1*^{A4V} HB9::GFP$^+$, un-sorting of healthy hESC (n=1), hiPSC (n=3), Isogenic control of *SOD1* (n=1), *C9ORF72* (n=6), *SOD1* (n=3), *TDP43* (n=3) and sporadic (n=5) derived sMN) were performed with an Agilent Accurate Mass 6230 TOF coupled with an Agilent 1290 Liquid Chromatography system using a Cogent Diamond Hydride Type C column (Microsolve Technologies, Long Branch, NJ, USA) with solvents and configuration as previously described[81]. An isocratic pump was used for continuous infusion of a reference mass solution to allow mass axis calibration. Detected ions were classified as metabolites based on unique accurate mass-retention time identifiers for masses showing the expected distribution of accompanying isotopologues. Metabolites were analyzed using Agilent Qualitative Analysis B.07.00 and Profinder B.08.00 software (Agilent Technologies, Santa Clara, CA, USA) with a mass tolerance of <0.005 Da. Standards of authentic chemicals of known amounts were mixed with bacterial lysates and analyzed to generate the standard curves used to quantify metabolite levels. All data obtained by metabolomics profiling were the average of at least two independent triplicates. Bioinformatics analysis was carried out using MetaboAnalyst v.4.0 (www.metaboanalyst.ca), which is a web-based available software for processing metabolomics data, and pathway mapping was performed on the basis of annotated Human metabolic pathways available in the Kyoto Encyclopedia of Genes and Genomes pathway database. Metabolomics data were analyzed by statistical analysis. The clustered heat map and hierarchical clustering trees were generated using Cluster 3.0 and Java Tree View 1.0. A univariate statistical analysis involving an unpaired t-test was

used to identify significant differences in the abundances of metabolites between each groups.

Transgenic mice & animal ethics

Hb9::GFP and ISL1::GFP mice were described previously[82,83]. The following mouse lines (25–30 g, 8–12 weeks old, male and female) were used for timed mating: C57BL/6J mice (Jackson Laboratory, Damul Science). For timed matings, a male mouse with two females were housed. Females were examined for vaginal plugs daily. The day when a vaginal plug was detected was designated embryonic day 0.5 (E0.5). All experiments used protocols approved by the Animal Care and Ethics Committees of the Gwangju Institute of Science and Technology (GIST, approval # GIST-2010-12) in accordance with the National Institutes of Health Guide for the Care and Use of Laboratory Animals. For efficacy assessment of the caffeic acid, B6.Cg-Tg(*SOD1*^{G93A})1Gur/J mice (Jackson Laboratory, Bar Harbor, ME, Stock# 002726) was used after in vitro fertilization (Macrogen, Seoul, Korea) and all the protocol was approved by the Institutional Animal Care and Use Committees of Dong-A University.

Animal housing

Mice were maintained on a 12:12 light cycle (lights on at 07:00) with water and food ad libitum and room temperature of 21–23°C and 50–60% humidity.

Mouse survival and efficacy evaluation

Caffeic acid (30 mg/kg) dissolved in PBS containing 10% ethanol or vehicle (PBS containing 10% ethanol) were orally administered 5 days/week from D60 to D120 of age. Three independent experiments were performed to evaluated the efficacy of caffeic acid. A total of 24 mice in each group (female=12, male=12) were used for evaluation of survival and behavioral assessments (Exp 1), and the same number of mice were used for histologic analyses (Exps 2 and 3). In the Exp 1, mice were monitored for neurological disease progression according to guide lines for preclinical animal research in ALS/MND[84]. The neurological score was followed as Score 0.5 as disease onset (first signs of tremor and hind-limb splay defects) and the end stage (Score 4) was determined as loss of righting reflex within 30s. Neurological scoring was monitored daily and mice at the end stage were euthanized. Kaplan-Meier curves was used to analyze age of onset and survival using Graphpad Prism7 (GraphPad Software, San Diego, CA). Motor coordination and muscle integrity were assessed weekly using a Rotarod apparatus and grip strength device (Panlab Harvard Apparatus, Barcelona, Spain). Tissue analyses were performed in the Exp 2 (n=14 for each group) and Exp 3 (n=10 for each group). They were anesthetized with euthanized isofluran at 16 wks (Exp 2) and 20 wks (Exp 3) of age then perfused with 4% paraformaldehyde in PBS. L4-L5 segments of spinal cord and motor cortex were serially cut with the cryostat into 20 μm sections then stained with 0.1% (w/v) cresyl violet stain solution. Motor neurons with larger than 25 μm of dimeter in Lamina IX of the ventral horn were counted using Image J software (National Institutes of Health, Bethesda, USA) program, and 10 sections per sample (n=10 for each group) were averaged. Activated astrocytes and microglia in the spinal cord were detected using rabbit anti-GFAP (abcam, ab7260, 1:500), rat anti-Iba1 (Wako, 019-19741, 1:500) for 10

sections per sample (n=10 for each group). The integrated density of fraction area in the ventral horn were measured using Image J software for quantification of activated astrocytes and microglia. Neuromuscular junction was analyzed in gastrocnemius muscle (30 μm) with anti-α-bungarotoxin (Alexa Fluor 488 conjugate, Invitrogen, B13422, 1:300) to label AChR and rabbit anti-Neurofilament H (Sigam-Aldrich, N4142, 1:2000), rabbit-Syanpsin-1 (Cell signaling, D12G5, 1:2000) to label axon terminals. Goat anti-rabbit Cy3 (Jackson, 111-165-003, 1:1000) was used as a secondary antibody. The innervated pretzel structures merged with two fluorescence were counted.

Whole mount staining

For whole mount immunostaining, E11.5 embryos were fixed in 4% PFA, permeabilized in PBS-T (1% Triton X-100 in PBS), blocked using blocking buffer (1% heat inactivated goat serum, 1% Triton X-100 in PBS) at 4°C. Embryos were incubated 3–5 days at 4°C with rabbit anti-GFP (Thermo Fisher, A-11122, 1:4000) primary antibody in blocking buffer. Fluorophore-conjugated secondary antibody (Alexa Fluor 488, Thermo Fisher, A-11034, 1:1000) was incubated for 1 day at 4°C, and images were captured using a Zeiss confocal microscope[85].

Fly stocks and culture

Flies were maintained on a cornmeal–molasses–yeast medium at room temperature (22 °C) with 60–65% humidity. The following *Drosophila* lines were obtained from the Bloomington Stock Center: *elav-GAL4*, *GMR-GAL4*, and *OK371-GAL4*. The *UAS-*$(G_4C_2)_3$ and *UAS-*$(G_4C_2)_{30}$ lines were obtained from Dr. Peng Jin's laboratory[43].

Fly eye degeneration experiment

UAS-$(G_4C_2)_{30}$ flies recombined with *GMR-Gal4* were selected as male parental flies for crossing (♀w^{1118} × ♂*GMR-Gal4; UAS-*$(G_4C_2)_{30}$/CyO). Overexpressing 30 hexanucleotide repeat (HRE) in all photoreceptors using *GMR-Gal4* causes eye degeneration in adult flies during aging. Eye degeneration scores were examined based on Dr. Paul Taylor's study[86]. Data of eye degeneration was quantified for the presence of: supernumerary inter-ommatidial bristles (IOBs), IOBs with abnormal orientation, necrotic patches, a decrease in size, retinal collapse, fusion of ommatidia, disorganization of ommatidial array and loss of pigmentation in adult male progeny. Points were added if: there was complete loss of IOBs (+1), more than 3 small or 1 large necrotic patch (+1), retinal collapse extended to the midline of the eye (+1) or beyond (+2), loss of ommatidial structure in less than 50% (+1) or more than 50% (+2) of the eye, and if pigmentation loss resulted in change of eye color from red to orange (+1) or pale orange/white (+2).

Fly survival experiment

UAS-$(G_4C_2)_{30}$ flies recombined with *OK371-Gal4* were selected as male parental flies for crossing (♀w^{1118} × ♂*OK371-Gal4; UAS-*$(G_4C_2)_{30}$/TM6B, GAL80). Overexpressing 30 HRE in fly motor neurons using *OK371-Gal4* causes lethality due to paralysis, preventing eclosion of the adult from the pupal case. According to Mendelian inheritance, the theoretical ratio of progenies with 30 HRE expressions from the above crossing is 50%.

A total of 100 adult flies were collected in each group. Survival rate was calculated as the ratio of the flies with 30 HRE that survive to adulthood to total adult flies and then divided by theoretical ratio 50%.

Statistics and Reproducibility

Each value is from at least 3 different experiments of multiple batches and (Extended Data Fig. 1L and 8G–H used samples for statistical analysis with 3 independent experiments from 1 batch) reported as mean ± SEM. Statistical differences between samples were analyzed by unpaired Student's t-test in GraphPad Prism 7 and indicated the p-value level with two-tailed in each legend. For statistical analysis of samples, to confirm our interest in such variability *in vitro*, we included several biological repeats from different donors and this information described in Supplement Data Table 2. Thus, every data was analyzed based on control or clinically non-affected cells without information of donor/genetic background. For animal experiment, we allocated 3 different groups (WT control, *SOD1* mutant (vehicle) and *SOD1* (drug)) and investigators were only aware of this, but we randomly allocated in each group and same number of male/female mice. All mice were monitored for neurological disease progression according to guide lines of preclinical animal research in ALS/MND and totally based on phenotypes without genetic information. For metabolomic pathway analysis in MetPA, we followed previously described method[87].

No statistical methods were used to pre-determine sample sizes but our sample sizes are similar to those reported in previous publications[21,65,69].

Extended Data

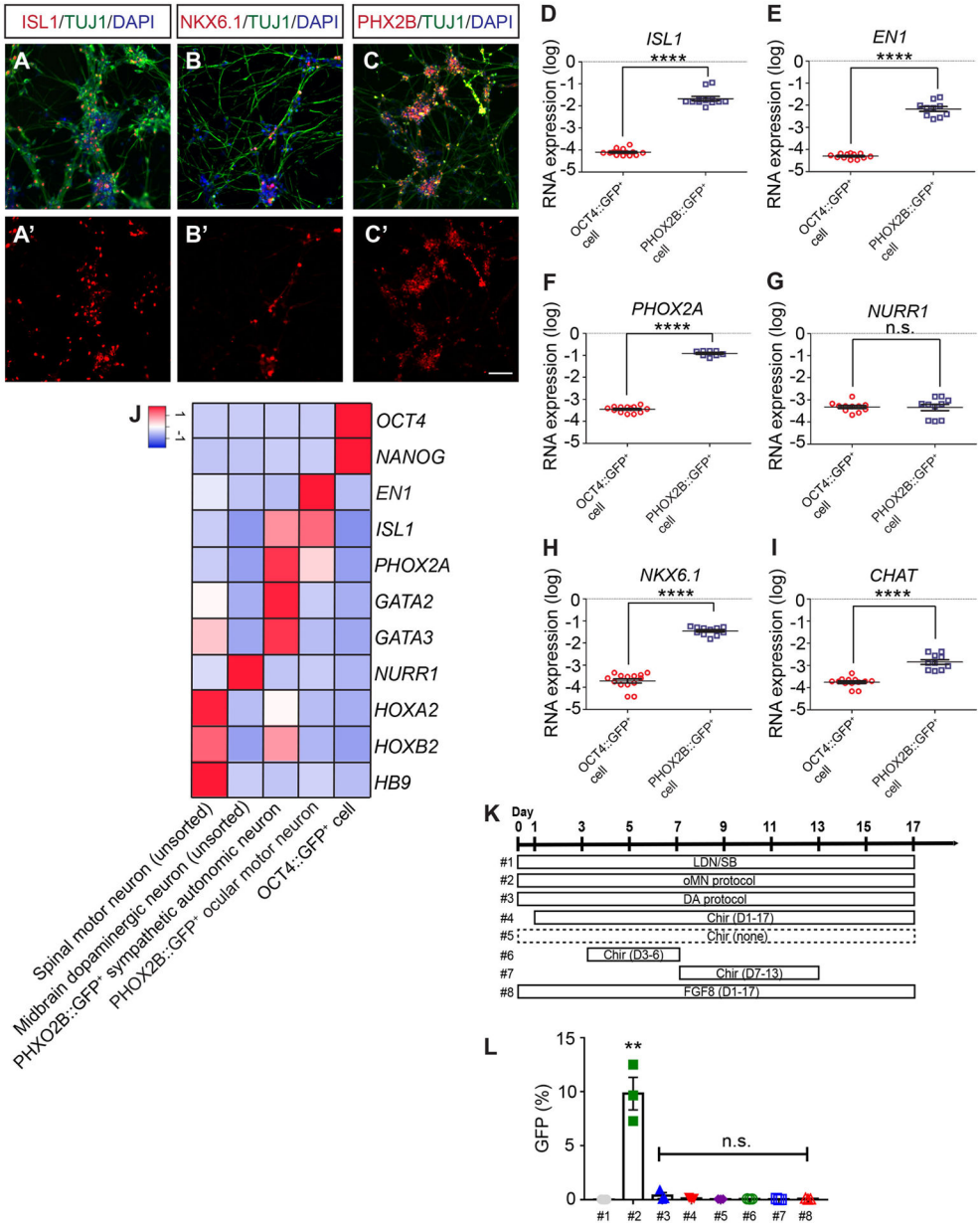

Extended Data Fig. 1. Characterization of transcripts in hiPSC-derived PHOX2B::GFP$^+$ oMN-like cells.

(A-C') Characterization of post-sorted PHOX2B::GFP$^+$ cells using ISL1, NKX6.1 and PHOX2B (red), and TUJ1 (green) antibodies. (D-I) qRT-PCR analysis shows enrichments of oMN specification transcripts (*ISL1, PHOX2A, NKX6.1* and *CHAT*) and midbrain regional transcript (*EN1*), but not mDA specification transcript (*NURR1*) after sorting (D14) (n=10 for each group from 3 independent batches; technical replicates; n.s.: not significant, ****P<0.0001 (p-value:<0.0001), two-tailed; unpaired student's t-test). (J) Heatmap presents characteristic marker expression of ES (OCT4::GFP), oMN-like (PHOX2B::GFP), sympathetic autonomic neuron (PHOX2B::GFP), mDA (unsorting) and sMN (unsorting)

(n=3 for each group, n means independent batches of differentiation; technical replicates). (K-L) Different schematic protocols to optimize oMN-like cell differentiation (K) and FACS results of PHOX2B::GFP^{+} (L) (n=3 for each groups (3 independent differentiation) from 1 batch; technical replicates; n.s.: not significant, **P<0.01 (0.0029), two-tailed; unpaired student's t-test). Scale bar: 100 μm, Error bars, mean ± SEM., PHX2B: PHOX2B.

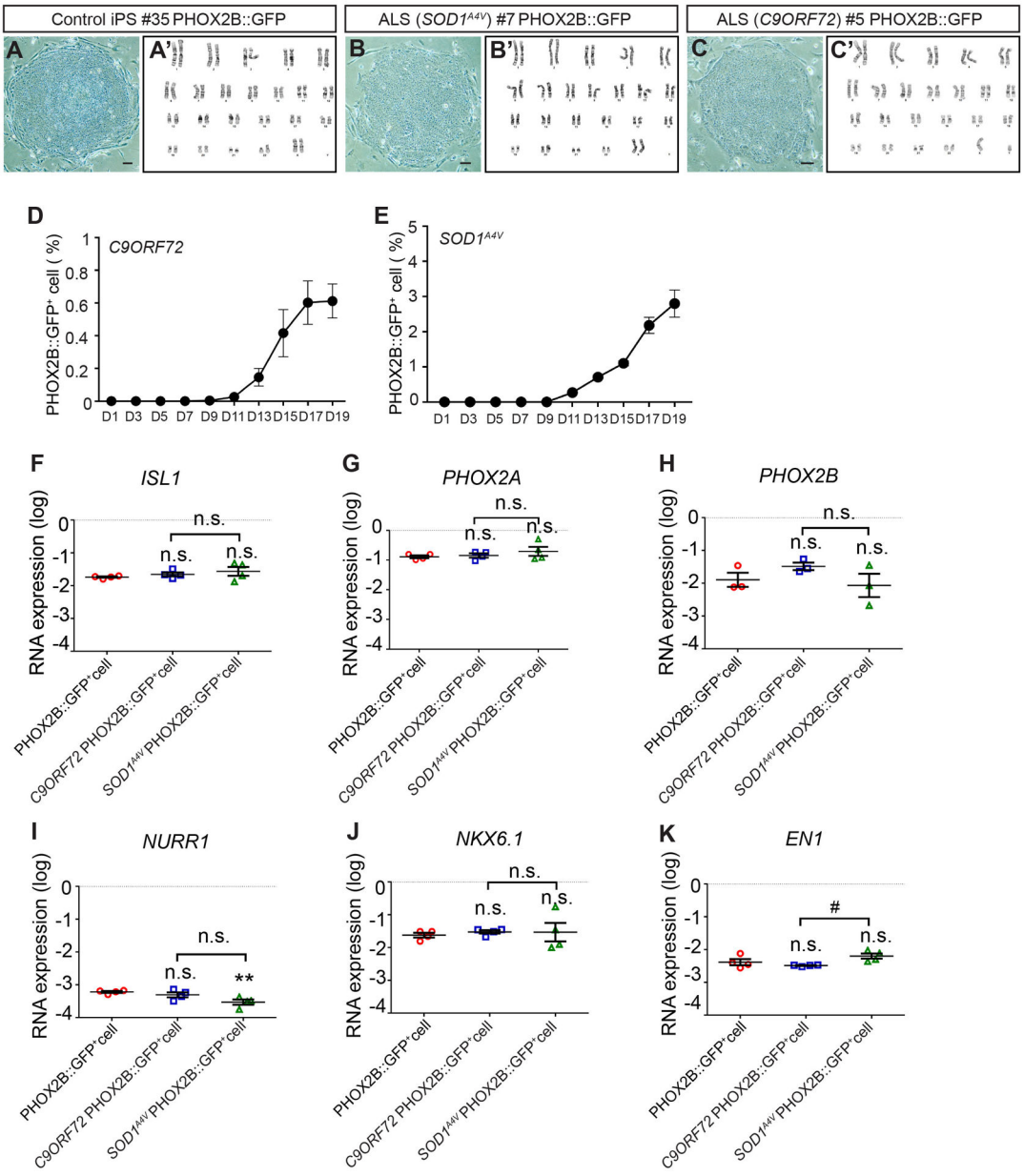

Extended Data Fig. 2. Generation of PHOX2B::GFP reporter line and oMN-like cell specification in *SOD1^{A4V}* and *C9ORF72* ALS lines.

(A-C') Representative images and karyotype results of control hiPSC, *SOD1^{A4V}* and *C9ORF72* PHOX2B::GFP reporter lines. (D-E) Time course GFP expression of oMN-like differentiation in *SOD1^{A4V}* and *C9ORF72* by FACS analysis (*SOD1^{A4V}*: n=3, *C9ORF72*: n=4 for each group; technical replicates; n means independent batches of

differentiation). (F-K) Enrichment of transcripts in post-sorted ES-derived and both ALS-derived PHOX2B::GFP^{+} is comparable for oMN (*ISL1, PHOX2A/B* and *NKX6.1*), midbrain specification (*EN1*) and mDA specification (*NURR1*) by qRT-PCR analysis (D14) (at least n=3 for each group, n means independent batches of differentiation (independent sorted samples); technical replicates; n.s.: not significant, #P < 0.05 (0.0104), **P<0.01 (0.0097), two-tailed; unpaired student's t-test). Scale bar: 100 μm, Error bars, mean ± SEM.

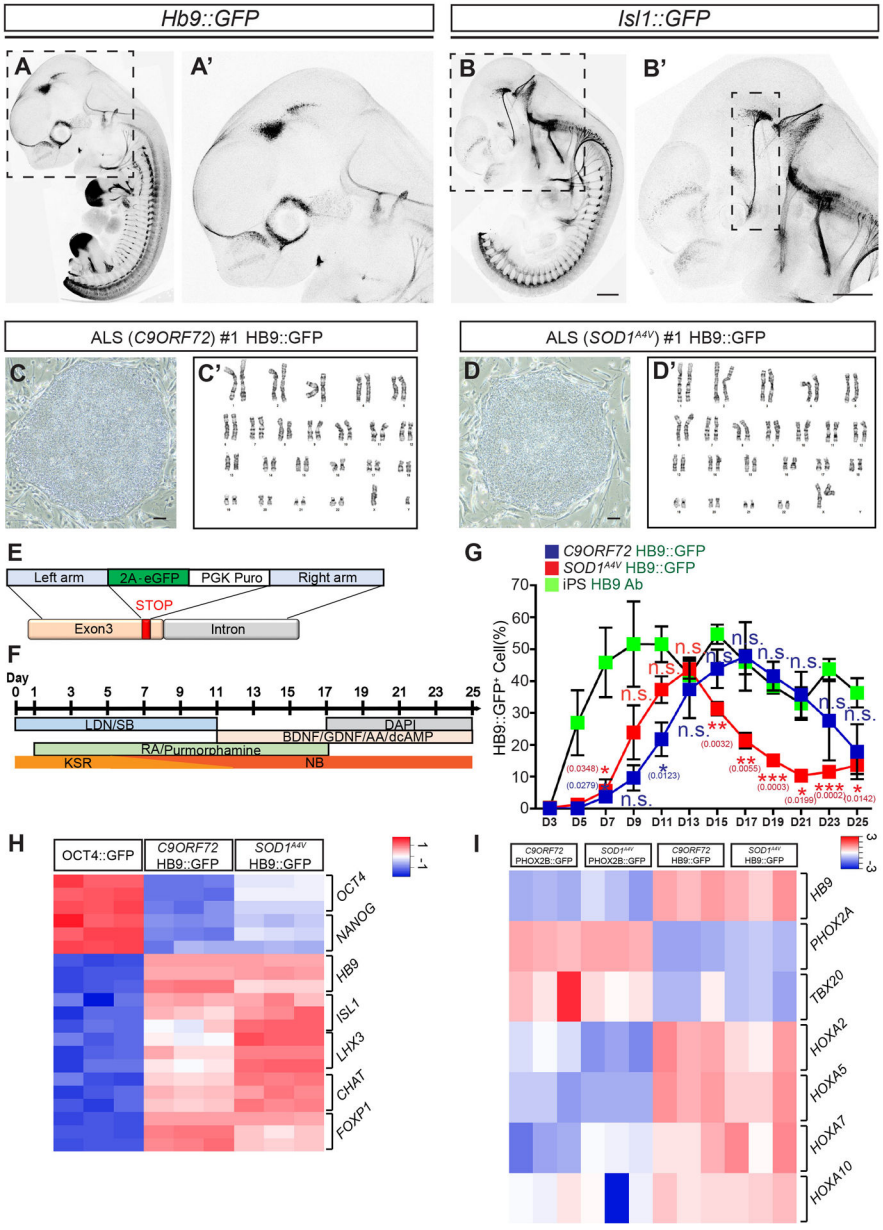

Extended Data Fig. 3. Generation of HB9::GFP reporter in *SOD1^{A4V}* and *C9ORF72* ALS lines.
(A-B') Wholemount GFP expression of Hb9 and Isl1 transgenic mouse at E11.5 embryo. Magnified view of images as indicated in (A') and (B'). (C-D) Representative images and karyotypes of *SOD1^{A4V}* and *C9ORF72* HB9B::GFP reporter lines. (E) Illustration of

HB9 gene targeting using CRISPR-Cas9 homologous recombination. (F) Schematic protocol of sMN cell differentiation. (G) Time course GFP expression of sMN differentiation in $SOD1^{A4V}$ / *C9ORF72* and HB9 antibody-stained cells of control hiPSC line by FACS analysis (at least n=3 for each group, n means independent batches of differentiation; technical replicates; n.s.: not significant, *P<0.05, **P<0.01, ***P<0.001, two-tailed; unpaired student's t-test; p-values are indicated in each graph). (H) Heatmap presents characteristic marker expression of ES (*OCT4* and *NANOG*) and sMN (*HB9, ISL1, LHX3*, *CHAT* and *FOXP1*) in post-sorted *OCT4::GFP*$^{+}$, $SOD1^{A4V}$ HB9::GFP^{+} and *C9ORF72* HB9::GFP^{+} cells by qRT-PCR (n=3 for each group, n means independent batches of differentiation; technical replicates). (I) A heatmap presents the gene expression levels of different spinal axis region markers (*HOXA2, A5, A7* and *A10*) and cell type specific makers (*HB9* for sMN and *PHOX2A* and *TBX20* for oMN-like) in post-sorted PHOX2B::GFP^{+} and HB9::GFP^{+} cells of $SOD1^{A4V}$ and *C9ORF72* ALS hiPSCs by qRT-PCR (n=3 for each group, n means independent batches of differentiation; technical replicates). Scale bars: 2000 μm (A-B') or 100 μm (C-D), Error bars: mean ± SEM.

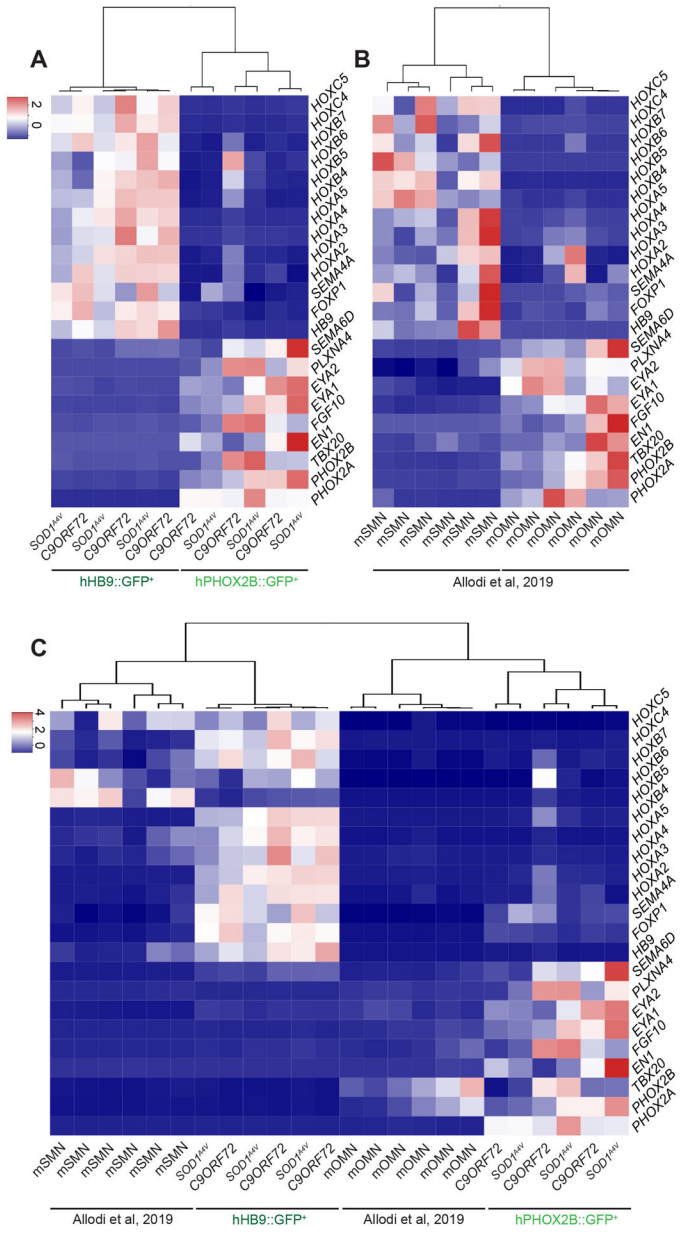

Extended Data Fig. 4. Validation of oMN and sMN population by comparing transcriptome profile with reference dataset.

(A-B) Heatmap shows differential expression levels of oMN- or sMN-specific genes in sorted HB9::GFP^{+} and PHOX2B::GFP^{+} of *SOD1*^{A4V} and *C9ORF72* ALS hiPSC lines (A), or reanalyzed mouse dataset from a previous literature (B). (C) Combined heatmap shows relative expression levels of oMN- or sMN-specific genes in sorted HB9::GFP^{+} and PHOX2B::GFP^{+} of *SOD1*^{A4V} and *C9ORF72* ALS hiPSC lines, and reanalyzed mouse dataset from a previous literature.

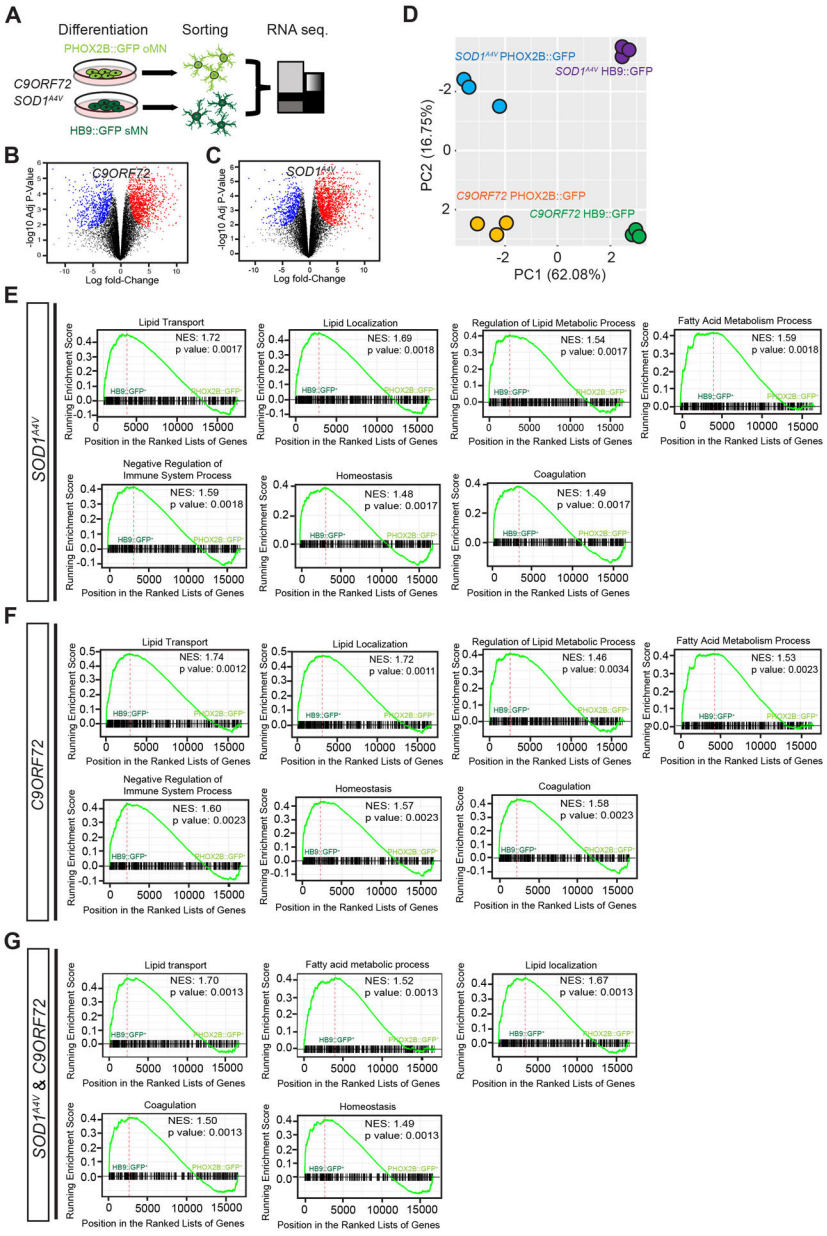

Extended Data Fig. 5. Transcriptome profiling reveals differences between PHOX2B::GFP$^+$ and HB9::GFP$^+$ cells in both *SOD1^{A4V}* and *C9ORF72* ALS lines.

(A) Illustration of transcriptome profiling of HB9::GFP$^+$ versus PHOX2B::GFP$^+$. (B-C) Volcano plots indicate a substantial transcriptomic difference between HB9::GFP and PHOX2B::GFP in both *SOD1^{A4V}* and *C9ORF72* ALS lines (n=3 for each group, n means independent batches of differentiation; technical replicates) (see Methods section for details). (D) Principal component analysis (PCA) plot represents distinct clustering between HB9::GFP and PHOX2B::GFP cell types-derived from both *SOD1^{A4V}* and *C9ORF72* ALS lines (n=3 for each group, n means independent batches of differentiation; technical replicates). (E-F) Gene set enrichment analysis (GSEA) plots show commonly over-represented GO terms of HB9::GFP$^+$ cells compared to PHOX2B::GFP$^+$ cells in both *SOD1^{A4V}* and *C9ORF72* ALS lines (n=3 for each group, n means independent batches of

differentiation; technical replicates). (G) Combined dataset of the two ALS lines consistently shows the same over-represented GO terms as observed in single ALS line datasets (n=3 for each group, n means independent batches of differentiation; technical replicates). p-value of the enrichment analysis was calculated using the Hypergeometric test (phyper function) which is equivalent to one-tailed Fisher's Exact test.

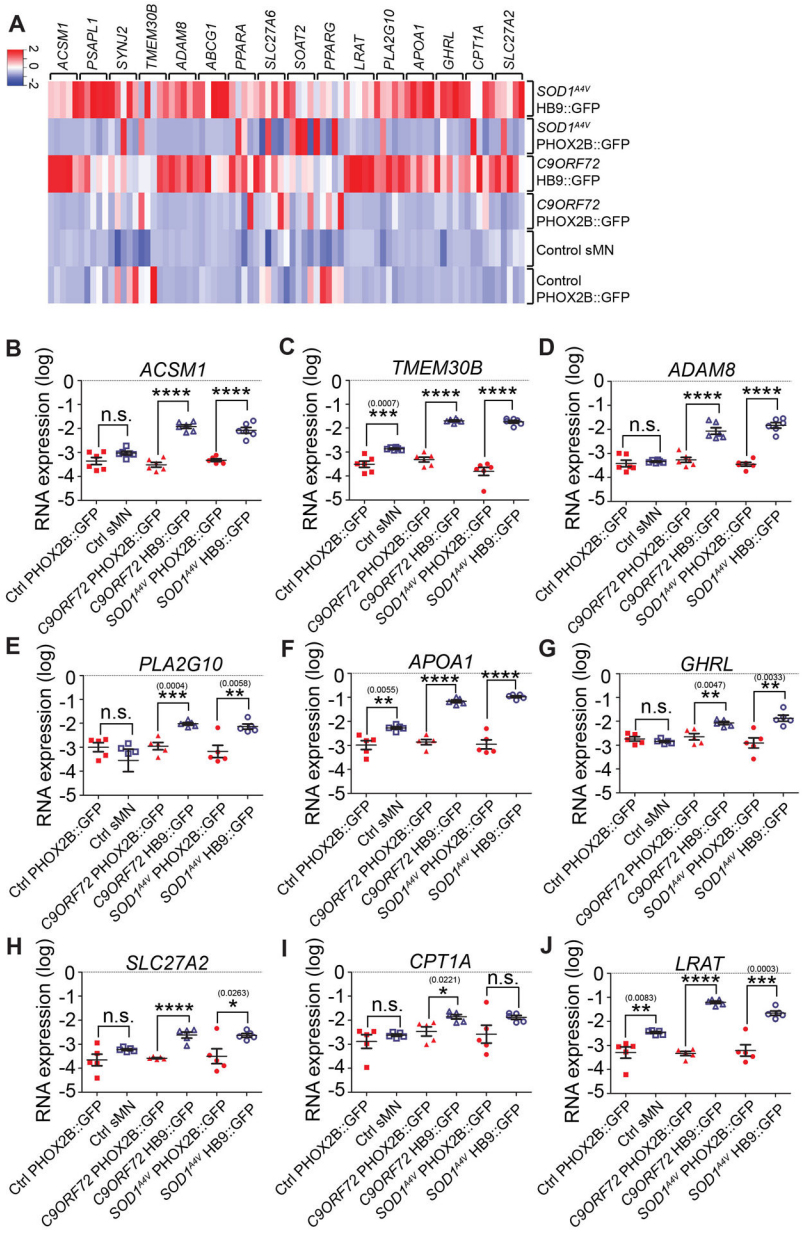

Extended Data Fig. 6. Verification of abnormal expression of lipid related transcripts in *SOD1^{A4V}* and *C9ORF72* ALS lines by qRT-PCR analysis.

(A) Heatmap shows enriched transcripts in sorted *HB9::GFP*$^{+}$ of *SOD1^{A4V}* and *C9ORF72,* but not sorted control and PHOX2B::GFP^{+}. (B-J) Individual plot indicates altered expression transcripts in post-sorted HB9::GFP^{+} of *SOD1^{A4V}* and *C9ORF72* (*P<0.05, **P<0.01, ***P<0.001, ****P<0.0001 (p-value:<0.0001), n.s.: not significant, two-tailed; unpaired

student's t-test, at least n=3 for each group, n means independent batches of differentiation; technical replicates; p-values are indicated in each graph). Error bars: mean ± SEM.

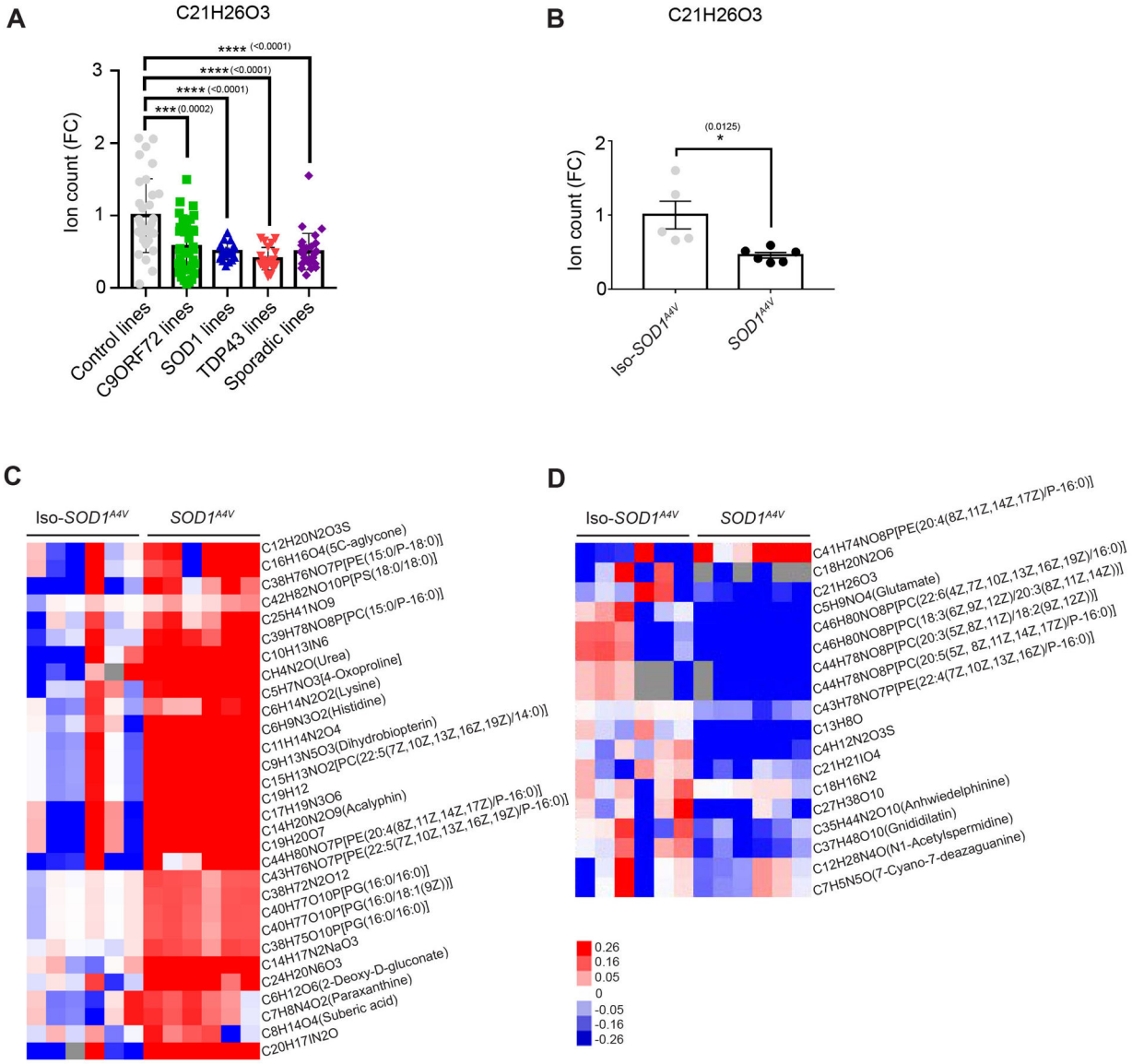

Extended Data Fig. 7. Common alteration of $C_{21}H_{26}O_3$ in multiple ALS lines and direct comparision of altered metabolic metabolites by metabolomics analysis in isogenic control of *SOD1*^{A4V} and *SOD1*^{A4V} ALS hiPSC lines.

(A-B) Ion count values present commonly down-regulated $C_{21}H_{26}O_3$ metabolic candidate in multiple ALS lines (A) and direct comparison of isogenic control of *SOD1*^{A4V} and *SOD1*^{A4V} lines (B) (*P<0.05, ***P<0.001, ****P<0.0001, n.s.: not significant, two-tailed; unpaired student's t-test; p-values are indicated in each graph; at least n=3 for each lines; technical replicates; n=1 hESC control, n=3 hiPSC control, n=1 isogenic control hiPSC of *SOD1*^{A4V}, n=6 *C9ORF72*, n=3 *SOD1*, n=3 *TDP43*, n=5 sporadic ALS hiPSC; biological replicates). (C-D) Heatmap shows the lists of selective metabolite candidate in isogenic

control of *SOD1*^{A4V} and *SOD1*^{A4V} ALS hiPSC lines (n=6 for each group, n means 6 independent differentiation from 2 batch; technical replicates). Error bars: mean ± SEM.

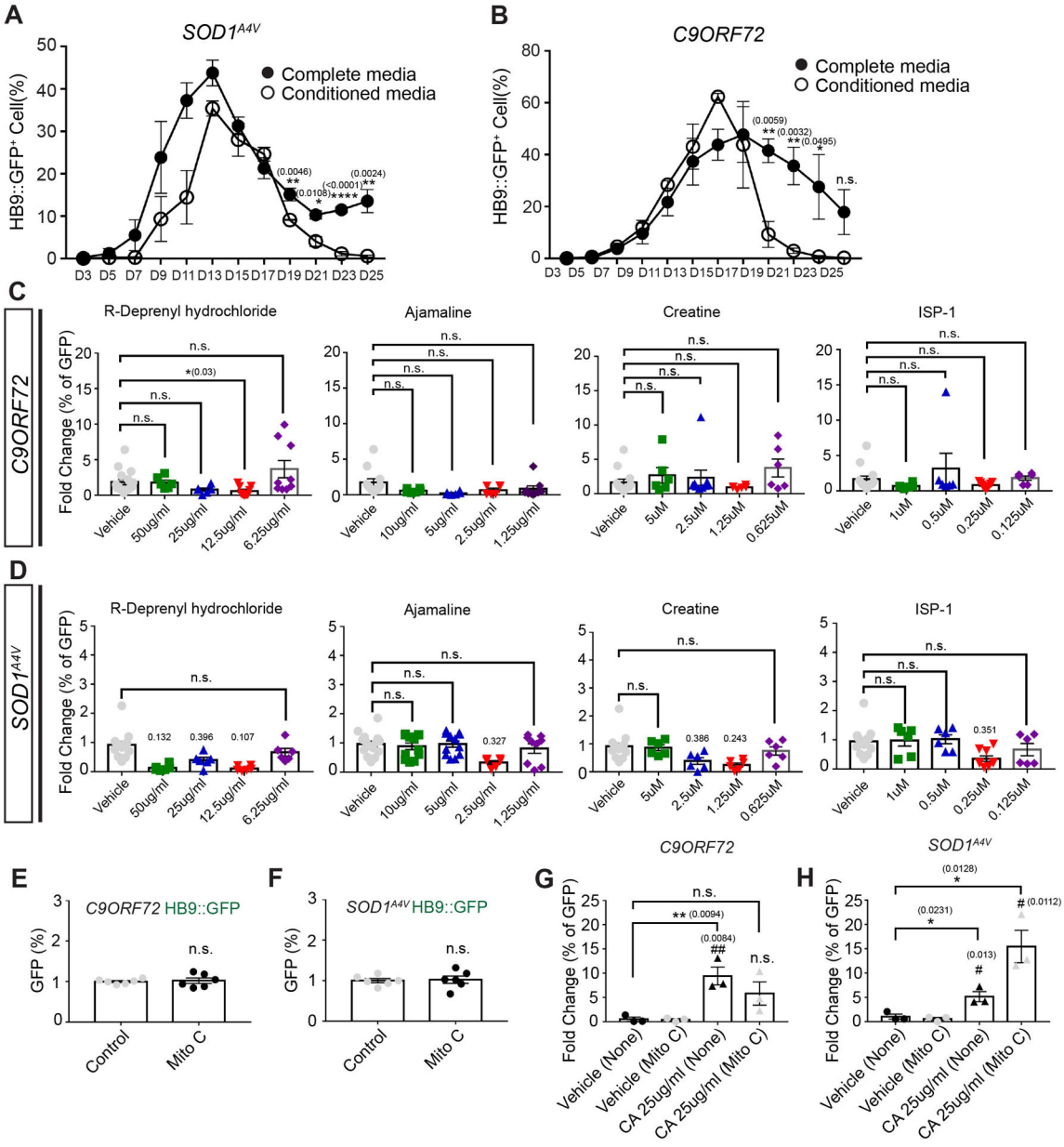

Extended Data Fig. 8. Caffeic acid exclusively rescues HB9::GFP^{+} cells in *SOD1*^{A4V} and *C9ORF72*.

(A-B) Experimental modification of media (conditioned media) shows enhanced HB9::GFP^{+} degeneration of *SOD1*^{A4V} and *C9ORF72* at D19 to D25 (complete media: n=3, conditioned media: n=4 for each ALS lines; technical replicates; n means independent batches of differentiation) (*P<0.05, **P<0.01, ****P<0.0001, two-tailed; unpaired student's t-test; p-values are indicated in each graph). (C-D) Results of compound tests in *SOD1*^{A4V} and *C9ORF72* HB9::GFP^{+} cells indicate comparable effects to control vehicle for each compound (R-Deprenyl hydrochloride, Ajamaline, Creatine and ISP-1) by FACS

analysis (Dot indicates different wells from at least 3 batches, at least n=6; technical replicates; *P<0.05, n.s.: not significant, unpaired student's t-test, two-tailed). (E-F) FACS results of HB9::GFP^{+} between control (non-treated) and mitomycin C treated (1 μg/ml, 1hr; D17 to D19 (2 days)) in *C9ORF72* and $SOD1^{A4V}$ ALS hiPSC lines (Dot indicates different wells from at least 2 batches, at least n=6; technical replicates; n.s.: not significant; unpaired student's t-test, two-tailed). (G-H) CA elevates the levels of HB9::GFP expression in the sMN culture of *C9ORF72* and $SOD1^{A4V}$ ALS hiPSC lines after mitomycin C treatment (n=3 for each group; n means 3 independent differentiation from 1 batch; technical replicates; n.s.: not significant; *,#, $p < 0.05$; **,##, $p < 0.01$ (*:compare with none treated vehicle, #: compare with mitomycin C treated vehicle), two-tailed; unpaired student's t-test; p-values are indicated in each graph). Error bars: mean ± SEM.

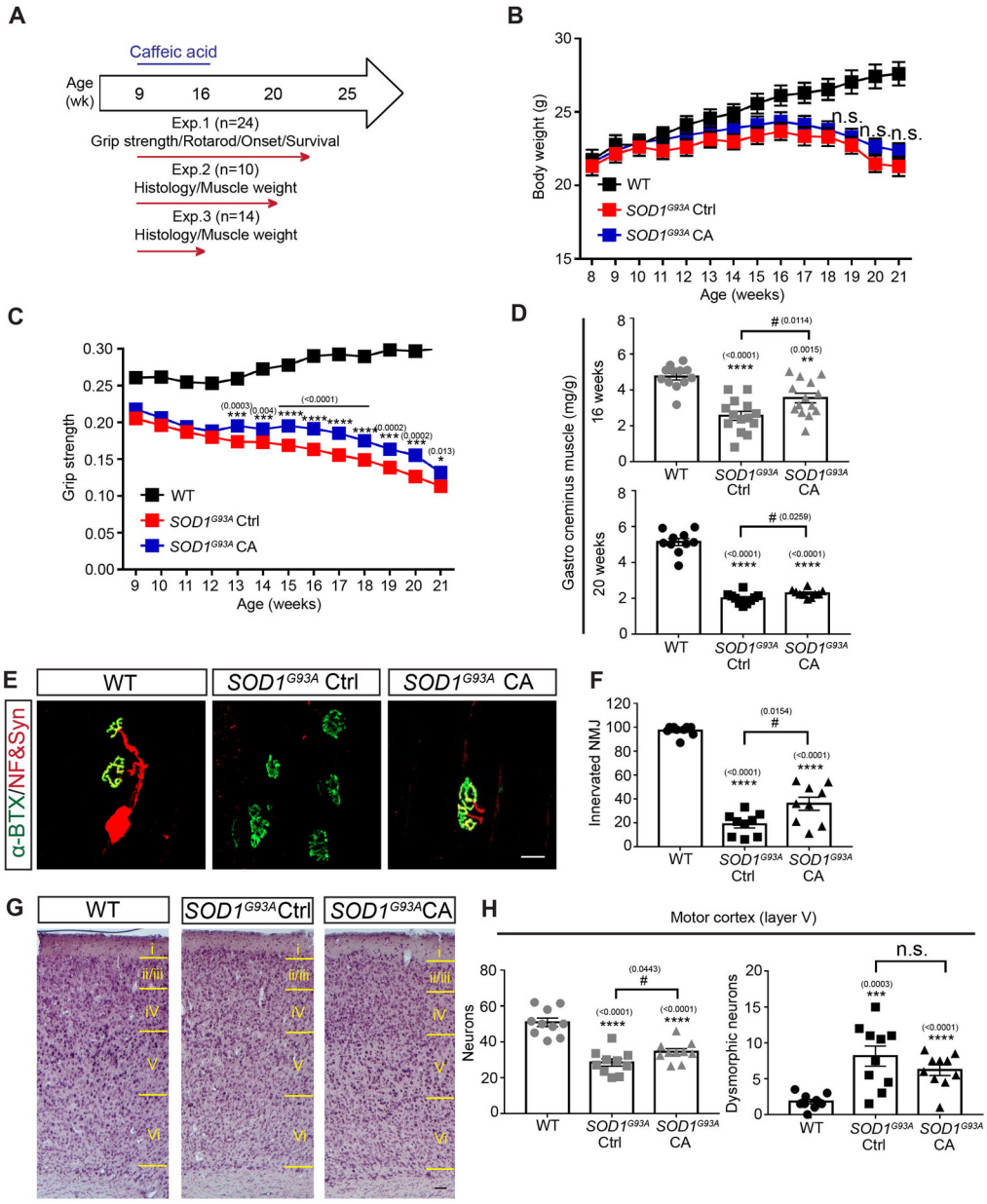

Extended Data Fig. 9. Caffeic acid alleviates disease pathogenesis in *SOD1*^{G93A} mice.

(A) Experimental scheme illustrating the CA administration and assessment of the efficacy. CA or vehicle (PBS with 10% ethanol) was administered to *SOD1*^{G93A} mice from D60 to D120 of age (5 days per week). (B) Changes of body weight monitored weekly (n=24 for each *SOD1*^{G93A} mice group; and n=20 for WT mice group). (C) Grip strength analysis. n=24 for each group. (D) The ratio of gastrocnemius muscle to body weight (mg/g) at the indicated time points. n=14 at 16 wks and n=10 at 20 wks for each group. (E) Neuromuscular junction visualized by α-bungarotoxin (α-BTX, green) and neurofilament H/synapsin (NF/Syn, red) in gastrocnemius muscle at 16 wks (Scale bar: 20 μm). (F) The ratio of innervated neuromuscular junction (NMJ). n=8 for each group. (G) Cresyl violet staining (Nissl staining) to visualize the pyramidal neuron (layer V) in motor cortex at 20

wks (Scale bar: 50 μm). (H) The number of pyramidal neurons and dysmorphic neurons in the layer V of motor cortex (n=10 for each group). (WT, wild-type mice; Ctrl, vehicle administered *SOD1*^{G93A} mice; CA, caffeic acid (30 mg/kg) administered *SOD1*^{G93A} mice; *,#, p < 0.05; **, p < 0.01;***, p < 0.001 and ****, p<0.0001., n.s.: not significant, two-tailed; unpaired student's t-test; p-values are indicated in each graph). Error bars: mean ± SEM.

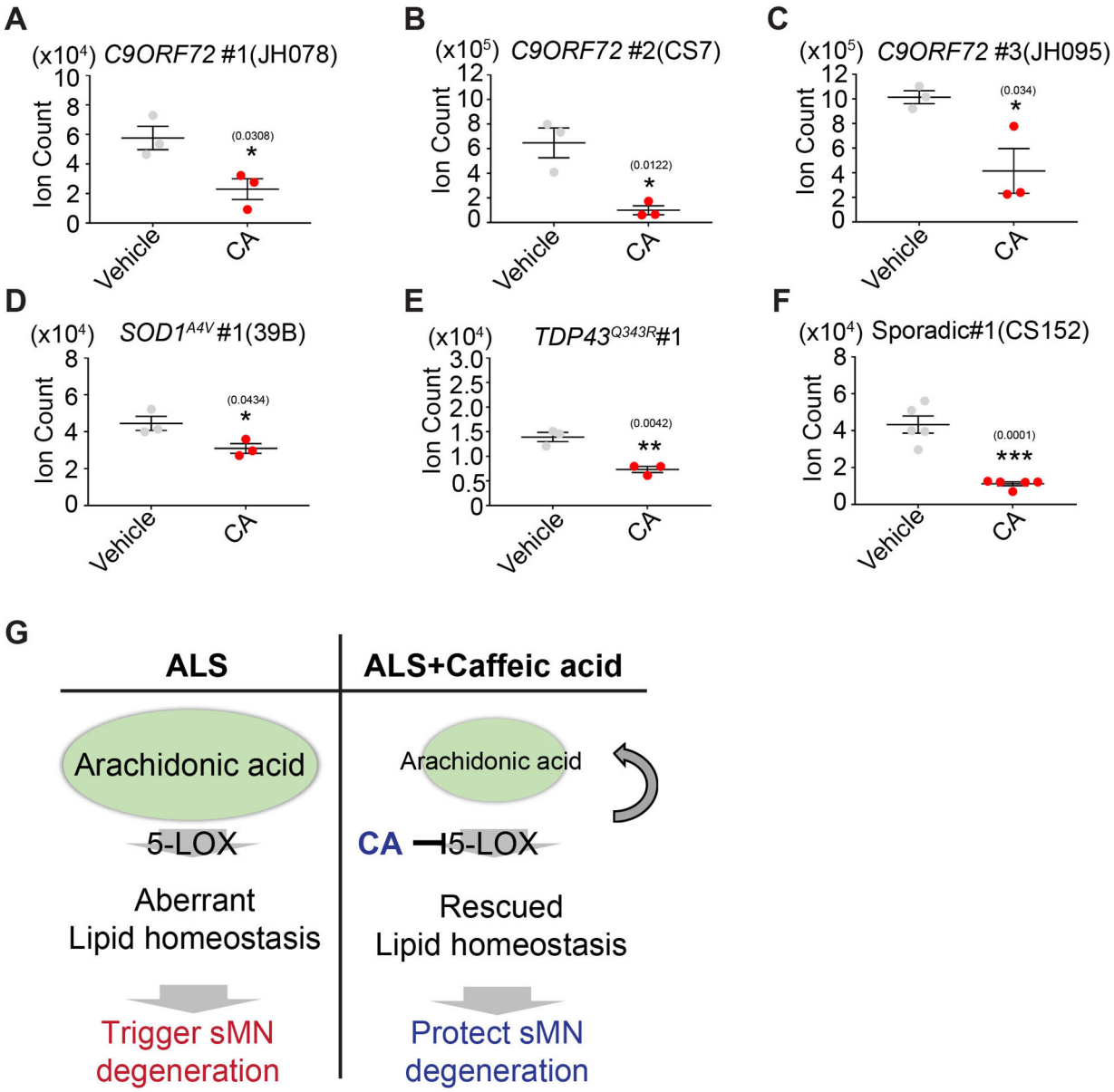

Extended Data Fig. 10. Caffeic acid rescues aberrant levels of arachidonic acid in the sMN culture of multiple ALS hiPC lines.

(A-F) Ion count value shows arachidonic acid level is down-regulated in post-treatment with 25 μg/ml CA at D11 to D17 of sMN differentiation of control and CA treated of ALS hiPSC lines (at least n=3 for each group; the cell line names are listed; technical replicates;

biological replicates; *P<0.05, **P<0.01, ***P<0.001, two-tailed; unpaired student's t-test). (G) Schematic model of this study. Error bars: mean ± SEM.

Supplementary Material

Refer to Web version on PubMed Central for supplementary material.

Acknowledgments

The authors thank H. Zhang at Flow Cytometry Core Facility (JHSPH), Haiping Hao and C. Talbot at Deep Sequencing Core Facility (JHU) for RNA sequencing data analysis. We also thank the Developmental Studies Hybridoma Bank for antibodies and Prof. Kevin Eggan (Harvard university) for sharing the isogenic control line.

Funding:

This work was supported by grants from the Donald E. & Delia Baxter Foundation (H.E.), Department of Molecular Microbiology and Immunology KSOM, USC (H.E.), Robert Packard Center for ALS Research (G.L.), the National Institutes of Health through R01NS093213 (G.L.), the Global Research Development Center Program from the National Research Foundation of Korea (NRF) (2017K1A4A3014959, G.L.), and Basic Research Program of NRF (2021R1A2C1007793, Y.B.H), and the Medical Research Center program (2016R1A5A2007009, Y.B.H) from NRF.

Data availability

The raw bulk RNA-sequencing data (Fig. 2/3D, Extended Data Fig. 4, 5 and Supplementary Data Fig. 4) are available at the Gene Expression Omnibus (GEO) under the accession code GSE132972 and GSE173115.

REFERENCES

1. Taylor JP, Brown RH Jr & Cleveland DW Decoding ALS: from genes to mechanism. Nature 539, 197 (2016). [PubMed: 27830784]
2. Tandan R & Bradley WG Amyotrophic lateral sclerosis: Part 1. Clinical features, pathology, and ethical issues in management. Annals of Neurology: Official Journal of the American Neurological Association and the Child Neurology Society 18, 271–280 (1985).
3. Saxena S & Caroni P Selective neuronal vulnerability in neurodegenerative diseases: from stressor thresholds to degeneration. Neuron 71, 35–48 (2011). [PubMed: 21745636]
4. Fujimori K et al. Modeling sporadic ALS in iPSC-derived motor neurons identifies a potential therapeutic agent. Nature medicine 24, 1579 (2018).
5. Kiskinis E et al. Pathways disrupted in human ALS motor neurons identified through genetic correction of mutant SOD1. Cell stem cell 14, 781–795 (2014). [PubMed: 24704492]
6. Klim JR et al. ALS-implicated protein TDP-43 sustains levels of STMN2, a mediator of motor neuron growth and repair. Nature neuroscience 22, 167 (2019). [PubMed: 30643292]
7. Melamed Z. e. et al. Premature polyadenylation-mediated loss of stathmin-2 is a hallmark of TDP-43-dependent neurodegeneration. Nature neuroscience 22, 180 (2019). [PubMed: 30643298]
8. Kaminski HJ, Richmonds CR, Kusner LL & Mitsumoto H Differential susceptibility of the ocular motor system to disease. Annals of the New York Academy of Sciences 956, 42–54 (2002). [PubMed: 11960792]
9. Cleveland DW & Rothstein JD From Charcot to Lou Gehrig: deciphering selective motor neuron death in ALS. Nature reviews neuroscience 2, 806 (2001). [PubMed: 11715057]
10. Kaplan A et al. Neuronal matrix metalloproteinase-9 is a determinant of selective neurodegeneration. Neuron 81, 333–348 (2014). [PubMed: 24462097]
11. Allodi I et al. Differential neuronal vulnerability identifies IGF-2 as a protective factor in ALS. Scientific reports 6, 25960 (2016). [PubMed: 27180807]

12. Mazzoni EO et al. Synergistic binding of transcription factors to cell-specific enhancers programs motor neuron identity. Nature neuroscience 16, 1219 (2013). [PubMed: 23872598]
13. Allodi I et al. Modeling motor neuron resilience in ALS using stem cells. Stem cell reports (2019).
14. Cutler RG, Pedersen WA, Camandola S, Rothstein JD & Mattson MP Evidence that accumulation of ceramides and cholesterol esters mediates oxidative stress–induced death of motor neurons in amyotrophic lateral sclerosis. Annals of Neurology: Official Journal of the American Neurological Association and the Child Neurology Society 52, 448–457 (2002).
15. Theofilopoulos S et al. Cholestenoic acids regulate motor neuron survival via liver X receptors. The Journal of clinical investigation 124, 4829–4842 (2014). [PubMed: 25271621]
16. Pattyn A, Hirsch M, Goridis C & Brunet J-F Control of hindbrain motor neuron differentiation by the homeobox gene Phox2b. Development 127, 1349–1358 (2000). [PubMed: 10704382]
17. Prakash N et al. Nkx6-1 controls the identity and fate of red nucleus and oculomotor neurons in the mouse midbrain. Development 136, 2545–2555 (2009). [PubMed: 19592574]
18. Hasan KB, Agarwala S & Ragsdale CW PHOX2A regulation of oculomotor complex nucleogenesis. Development 137, 1205–1213 (2010). [PubMed: 20215354]
19. Deng Q et al. Specific and integrated roles of Lmx1a, Lmx1b and Phox2a in ventral midbrain development. Development 138, 3399–3408 (2011). [PubMed: 21752929]
20. Nakano M et al. Homozygous mutations in ARIX (PHOX2A) result in congenital fibrosis of the extraocular muscles type 2. Nature genetics 29, 315 (2001). [PubMed: 11600883]
21. Oh Y et al. Functional coupling with cardiac muscle promotes maturation of hPSC-derived sympathetic neurons. Cell Stem Cell 19, 95–106 (2016). [PubMed: 27320040]
22. Kriks S et al. Dopamine neurons derived from human ES cells efficiently engraft in animal models of Parkinson's disease. Nature 480, 547 (2011). [PubMed: 22056989]
23. Tang M, Luo SX, Tang V & Huang EJ Temporal and spatial requirements of Smoothened in ventral midbrain neuronal development. Neural development 8, 8 (2013). [PubMed: 23618354]
24. Danielian PS & McMahon AP Engrailed-1 as a target of the Wnt-1 signalling pathway in vertebrate midbrain development. Nature 383, 332 (1996). [PubMed: 8848044]
25. Tsarovina K et al. Essential role of Gata transcription factors in sympathetic neuron development. Development 131, 4775–4786 (2004). [PubMed: 15329349]
26. Thaler J et al. Active suppression of interneuron programs within developing motor neurons revealed by analysis of homeodomain factor HB9. Neuron 23, 675–687 (1999). [PubMed: 10482235]
27. Song M-R et al. Islet-to-LMO stoichiometries control the function of transcription complexes that specify motor neuron and V2a interneuron identity. Development 136, 2923–2932 (2009). [PubMed: 19666821]
28. Lewcock JW, Genoud N, Lettieri K & Pfaff SL The ubiquitin ligase Phr1 regulates axon outgrowth through modulation of microtubule dynamics. Neuron 56, 604–620 (2007). [PubMed: 18031680]
29. Guidato S, Barrett C & Guthrie S Patterning of motor neurons by retinoic acid in the chick embryo hindbrain in vitro. Molecular and Cellular Neuroscience 23, 81–95 (2003). [PubMed: 12799139]
30. Calder EL et al. Retinoic acid-mediated regulation of GLI3 enables efficient motoneuron derivation from human ESCs in the absence of extrinsic SHH activation. Journal of Neuroscience 35, 11462–11481 (2015). [PubMed: 26290227]
31. Allodi I et al. Modeling motor neuron resilience in ALS using stem cells. Stem cell reports 12, 1329–1341 (2019). [PubMed: 31080111]
32. Hedlund E, Karlsson M, Osborn T, Ludwig W & Isacson O Global gene expression profiling of somatic motor neuron populations with different vulnerability identify molecules and pathways of degeneration and protection. Brain 133, 2313–2330 (2010). [PubMed: 20826431]
33. Valbuena GN et al. Metabolomic analysis reveals increased aerobic glycolysis and amino acid deficit in a cellular model of amyotrophic lateral sclerosis. Molecular neurobiology 53, 2222–2240 (2016). [PubMed: 25963727]
34. Xia J & Wishart DS Using MetaboAnalyst 3.0 for comprehensive metabolomics data analysis. Current protocols in bioinformatics 55, 14.10. 11–14.10. 91 (2016).

35. Lawton KA et al. Plasma metabolomic biomarker panel to distinguish patients with amyotrophic lateral sclerosis from disease mimics. Amyotrophic Lateral Sclerosis and Frontotemporal Degeneration 15, 362–370 (2014). [PubMed: 24984169]
36. Jatana M et al. Inhibition of NF-κB activation by 5-lipoxygenase inhibitors protects brain against injury in a rat model of focal cerebral ischemia. Journal of neuroinflammation 3, 12 (2006). [PubMed: 16689995]
37. Häfner A-K, Kahnt AS & Steinhilber D Beyond leukotriene formation–the noncanonical functions of 5-lipoxygenase. Prostaglandins & other lipid mediators (2019).
38. Cao Y, Pearman AT, Zimmerman GA, McIntyre TM & Prescott SM Intracellular unesterified arachidonic acid signals apoptosis. Proceedings of the National Academy of Sciences 97, 11280–11285 (2000).
39. Rizzo MT et al. Induction of apoptosis by arachidonic acid in chronic myeloid leukemia cells. Cancer research 59, 5047–5053 (1999). [PubMed: 10519422]
40. Yang JQ, Zhou QX, Liu BZ & He BC Protection of Mouse Brain from Aluminum-induced Damage by Caffeic Acid. CNS neuroscience & therapeutics 14, 10–16 (2008). [PubMed: 18482095]
41. Bishayee K & Khuda-Bukhsh AR 5-lipoxygenase antagonist therapy: a new approach towards targeted cancer chemotherapy. Acta Biochim Biophys Sin 45, 709–719 (2013). [PubMed: 23752617]
42. Pergola C & Werz O 5-Lipoxygenase inhibitors: a review of recent developments and patents. Expert opinion on therapeutic patents 20, 355–375 (2010). [PubMed: 20180620]
43. Xu Z et al. Expanded GGGGCC repeat RNA associated with amyotrophic lateral sclerosis and frontotemporal dementia causes neurodegeneration. Proceedings of the National Academy of Sciences 110, 7778–7783 (2013).
44. Abdel-Khalik J et al. Defective cholesterol metabolism in amyotrophic lateral sclerosis. Journal of lipid research 58, 267–278 (2017). [PubMed: 27811233]
45. An D et al. Stem cell-derived cranial and spinal motor neurons reveal proteostatic differences between ALS resistant and sensitive motor neurons. eLife 8, e44423 (2019). [PubMed: 31157617]
46. Kuehne A et al. Acute activation of oxidative pentose phosphate pathway as first-line response to oxidative stress in human skin cells. Molecular cell 59, 359–371 (2015). [PubMed: 26190262]
47. Patra KC & Hay N The pentose phosphate pathway and cancer. Trends in biochemical sciences 39, 347–354 (2014). [PubMed: 25037503]
48. Lopez-Gonzalez R et al. Poly (GR) in C9ORF72-related ALS/FTD compromises mitochondrial function and increases oxidative stress and DNA damage in iPSC-derived motor neurons. Neuron 92, 383–391 (2016). [PubMed: 27720481]
49. Andrus PK, Fleck TJ, Gurney ME & Hall ED Protein oxidative damage in a transgenic mouse model of familial amyotrophic lateral sclerosis. Journal of neurochemistry 71, 2041–2048 (1998). [PubMed: 9798929]
50. Dodge JC et al. Glycosphingolipids are modulators of disease pathogenesis in amyotrophic lateral sclerosis. Proceedings of the National Academy of Sciences 112, 8100–8105 (2015).
51. Dodge JC et al. Neutral lipid cacostasis contributes to disease pathogenesis in amyotrophic lateral sclerosis. Journal of Neuroscience 40, 9137–9147 (2020). [PubMed: 33051352]
52. Andrés-Benito P et al. Lipid alterations in human frontal cortex in ALS-FTLD-TDP43 proteinopathy spectrum are partly related to peroxisome impairment. Neuropathology and Applied Neurobiology 47, 544–563 (2021). [PubMed: 33332650]
53. Mohassel P et al. Childhood amyotrophic lateral sclerosis caused by excess sphingolipid synthesis. Nature Medicine, 1–8 (2021).
54. Das UN Arachidonic acid in health and disease with focus on hypertension and diabetes mellitus: A review. Journal of advanced research 11, 43–55 (2018). [PubMed: 30034875]
55. Solomonov Y, Hadad N & Levy R Reduction of cytosolic phospholipase A 2 α upregulation delays the onset of symptoms in SOD1G93A mouse model of amyotrophic lateral sclerosis. Journal of neuroinflammation 13, 1–12 (2016). [PubMed: 26728181]
56. Tallima H & El Ridi R Arachidonic acid: physiological roles and potential health benefits–a review. Journal of advanced research 11, 33–41 (2018). [PubMed: 30034874]

57. Blasco H et al. Lipidomics reveals cerebrospinal-fluid signatures of ALS. Scientific reports 7, 1–10 (2017). [PubMed: 28127051]
58. Chaves-Filho AB et al. Alterations in lipid metabolism of spinal cord linked to amyotrophic lateral sclerosis. Scientific reports 9, 1–14 (2019). [PubMed: 30626917]
59. West M et al. The arachidonic acid 5-lipoxygenase inhibitor nordihydroguaiaretic acid inhibits tumor necrosis factor α activation of microglia and extends survival of G93A-SOD1 transgenic mice. Journal of neurochemistry 91, 133–143 (2004). [PubMed: 15379894]
60. Ran FA et al. Genome engineering using the CRISPR-Cas9 system. Nature protocols 8, 2281 (2013). [PubMed: 24157548]
61. Hockemeyer D et al. Genetic engineering of human pluripotent cells using TALE nucleases. Nature biotechnology 29, 731 (2011).
62. Mali P et al. RNA-guided human genome engineering via Cas9. Science 339, 823–826 (2013). [PubMed: 23287722]
63. Gendron TF et al. Poly (GP) proteins are a useful pharmacodynamic marker for C9ORF72-associated amyotrophic lateral sclerosis. Science translational medicine 9, eaai7866 (2017). [PubMed: 28356511]
64. Almad AA et al. Connexin 43 in astrocytes contributes to motor neuron toxicity in amyotrophic lateral sclerosis. Glia 64, 1154–1169 (2016). [PubMed: 27083773]
65. Choi IY et al. Concordant but varied phenotypes among Duchenne muscular dystrophy patient-specific myoblasts derived using a human iPSC-based model. Cell reports 15, 2301–2312 (2016). [PubMed: 27239027]
66. Thomson JA et al. Embryonic stem cell lines derived from human blastocysts. science 282, 1145–1147 (1998). [PubMed: 9804556]
67. Riera M et al. Establishment and characterization of an iPSC line (FRIMOi001-A) derived from a retinitis pigmentosa patient carrying PDE6A mutations. Stem cell research 35, 101385 (2019). [PubMed: 30685614]
68. Coyne AN et al. G4C2 repeat RNA initiates a POM121-mediated reduction in specific nucleoporins in C9orf72 ALS/FTD. Neuron 107, 1124–1140. e1111 (2020). [PubMed: 32673563]
69. Lee G et al. Modelling pathogenesis and treatment of familial dysautonomia using patient-specific iPSCs. Nature 461, 402 (2009). [PubMed: 19693009]
70. Chambers SM et al. Highly efficient neural conversion of human ES and iPS cells by dual inhibition of SMAD signaling. Nature biotechnology 27, 275 (2009).
71. Qi Y et al. Combined small-molecule inhibition accelerates the derivation of functional cortical neurons from human pluripotent stem cells. Nature biotechnology 35, 154 (2017).
72. Lee H et al. Slit and Semaphorin signaling governed by Islet transcription factors positions motor neuron somata within the neural tube. Experimental neurology 269, 17–27 (2015). [PubMed: 25843547]
73. Pattyn A, Morin X, Cremer H, Goridis C & Brunet J-F Expression and interactions of the two closely related homeobox genes Phox2a and Phox2b during neurogenesis. Development 124, 4065–4075 (1997). [PubMed: 9374403]
74. Ng S-Y et al. Genome-wide RNA-Seq of human motor neurons implicates selective ER stress activation in spinal muscular atrophy. Cell stem cell 17, 569–584 (2015). [PubMed: 26321202]
75. Dobin A et al. STAR: ultrafast universal RNA-seq aligner. Bioinformatics 29, 15–21 (2013). [PubMed: 23104886]
76. Robinson MD, McCarthy DJ & Smyth GK edgeR: a Bioconductor package for differential expression analysis of digital gene expression data. Bioinformatics 26, 139–140 (2010). [PubMed: 19910308]
77. Law CW, Chen Y, Shi W & Smyth GK voom: Precision weights unlock linear model analysis tools for RNA-seq read counts. Genome biology 15, R29 (2014). [PubMed: 24485249]
78. McCarthy DJ & Smyth GK Testing significance relative to a fold-change threshold is a TREAT. Bioinformatics 25, 765–771 (2009). [PubMed: 19176553]

79. Subramanian A et al. Gene set enrichment analysis: a knowledge-based approach for interpreting genome-wide expression profiles. Proceedings of the National Academy of Sciences 102, 15545–15550 (2005).

80. Yu G, Wang L-G, Han Y & He Q-Y clusterProfiler: an R package for comparing biological themes among gene clusters. Omics: a journal of integrative biology 16, 284–287 (2012). [PubMed: 22455463]

81. Eoh H & Rhee KY Multifunctional essentiality of succinate metabolism in adaptation to hypoxia in Mycobacterium tuberculosis. Proceedings of the National Academy of Sciences 110, 6554–6559 (2013).

82. Lee S-K, Jurata LW, Funahashi J, Ruiz EC & Pfaff SL Analysis of embryonic motoneuron gene regulation: derepression of general activators function in concert with enhancer factors. Development 131, 3295–3306 (2004). [PubMed: 15201216]

83. Bai G et al. Presenilin-dependent receptor processing is required for axon guidance. Cell 144, 106–118 (2011). [PubMed: 21215373]

84. Ludolph AC et al. Guidelines for preclinical animal research in ALS/MND: A consensus meeting. Amyotrophic Lateral Sclerosis 11, 38–45 (2010). [PubMed: 20184514]

85. Kim K-T et al. ISL1-based LIM complexes control Slit2 transcription in developing cranial motor neurons. Scientific reports 6, 36491 (2016). [PubMed: 27819291]

86. Ritson GP et al. TDP-43 mediates degeneration in a novel Drosophila model of disease caused by mutations in VCP/p97. Journal of Neuroscience 30, 7729–7739 (2010). [PubMed: 20519548]

87. Xia J & Wishart DS MetPA: a web-based metabolomics tool for pathway analysis and visualization. Bioinformatics 26, 2342–2344 (2010). [PubMed: 20628077]

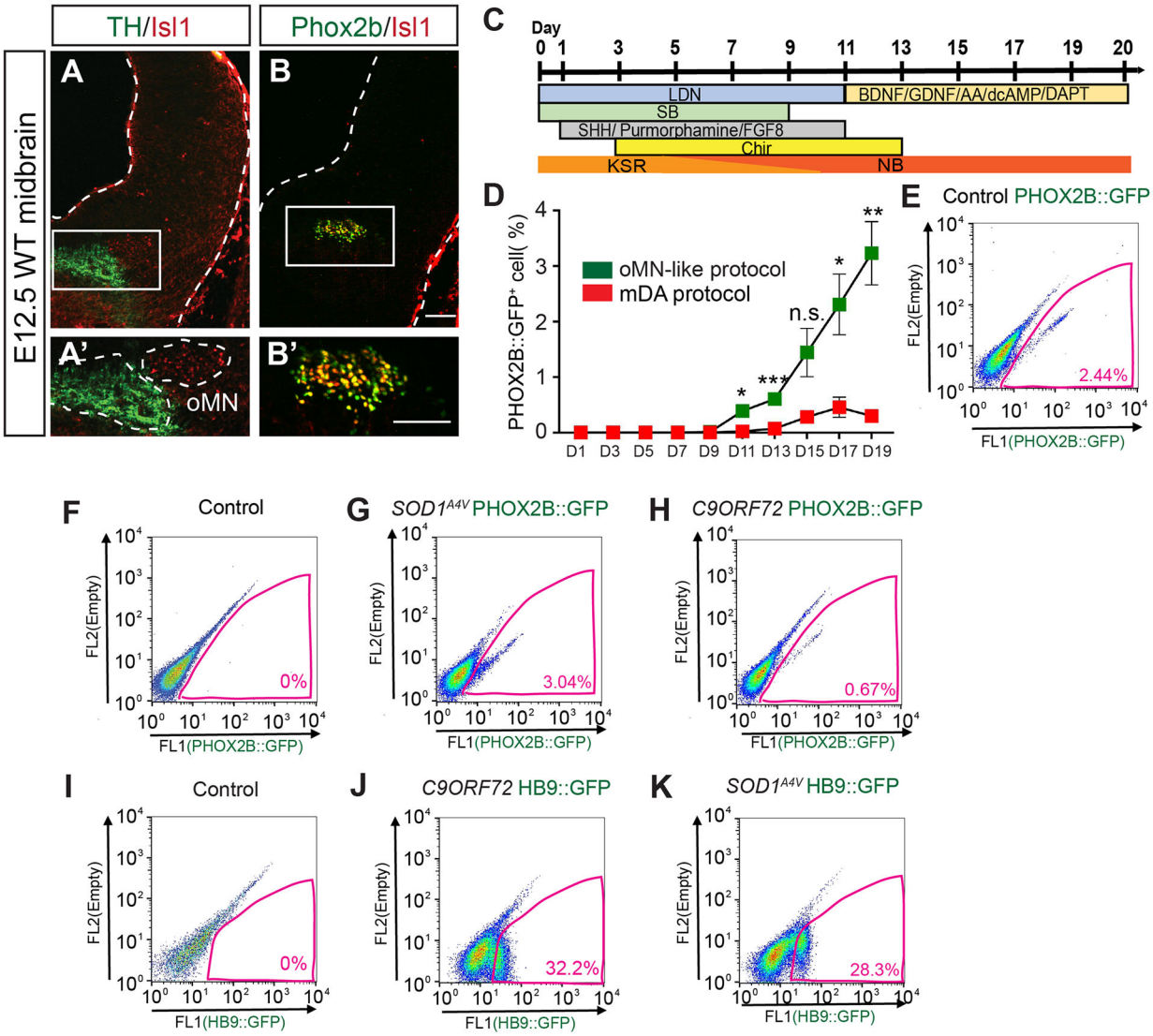

Fig. 1. Differentiation of PHOX2B::GFP$^+$ and HB9::GFP$^+$ neurons.

(A-B') Identification of neuronal subtypes in mouse midbrain using Isl1 and Phox2b for oMN, and TH for mDA. (C) Schematic protocol of oMN-like cell differentiation. (D) Time course comparison of PHOX2B::GFP$^+$ expression between oMN-like and mDA protocol by FACS (oMN-like: n=10, mDA: n=5, n means independent batches of differentiation; *P<0.05 (D11: 0.0173, D17: 0.037), **P<0.01 (D19: 0.0035), ***P<0.001 (D13: 0.0007), n.s.: not significant, two-tailed; unpaired student's t-test). (E-K) Representative FACS plot of PHOX2B::GFP reporter line for oMN-like cell differentiation in healthy control, *SOD1^{A4V}* and *C9ORF72* lines (E-H) and HB9::GFP reporter line for sMN differentiation in *SOD1^{A4V}* and *C9ORF72* lines (I-K). Scale bars, 100 μm, Error bars, mean ± SEM. oMN, ocular motor neuron. sMN, spinal motor neuron. mDA, midbrain dopaminergic neuron. TH, tyrosine hydroxylase.

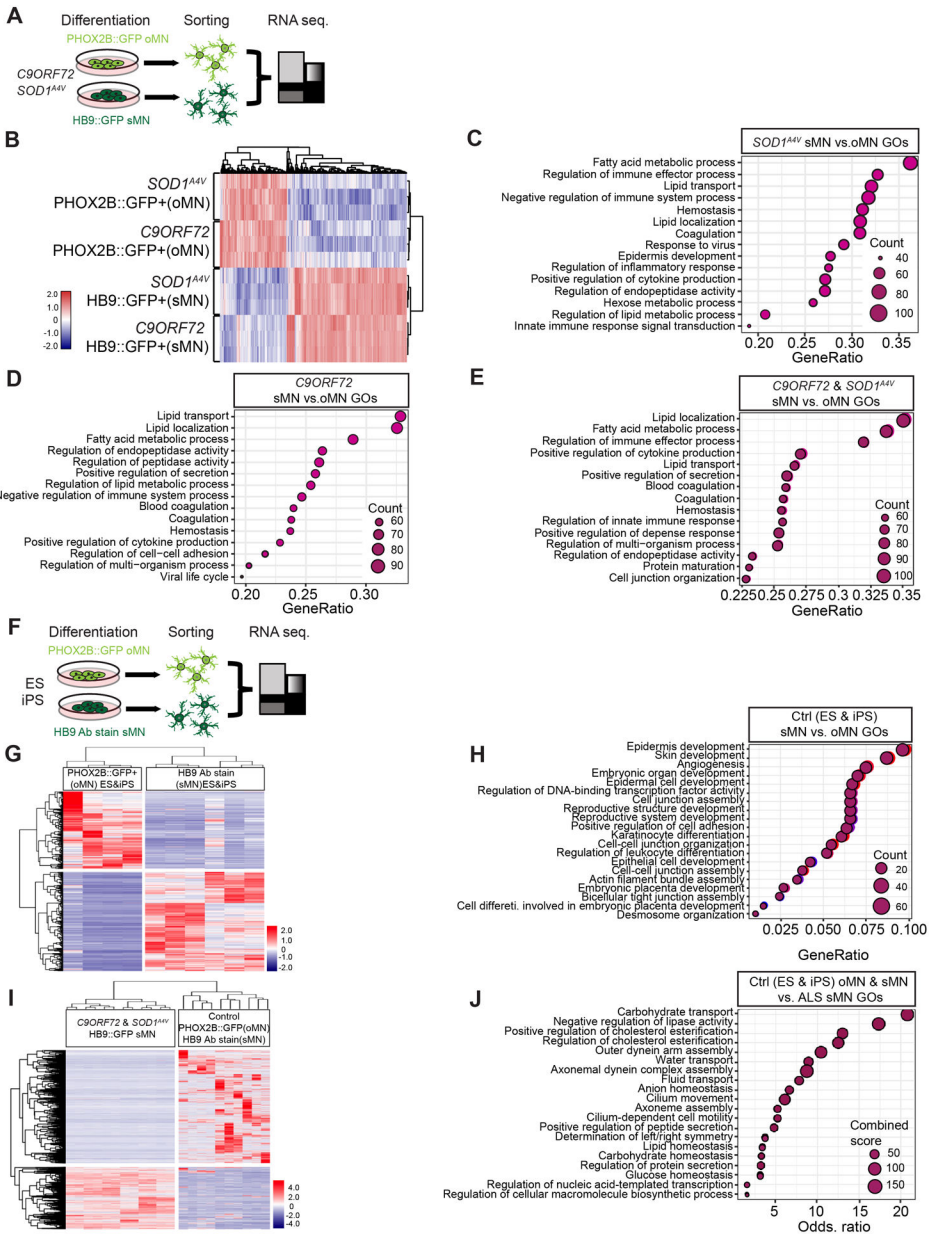

Fig. 2. Genome-wide RNA sequencing analysis reveals aberrant lipid metabolism after comparison between post-sorted HB9::GFP$^+$ and PHOX2B::GFP$^+$ in *SOD1^{A4V}* and *C9ORF72* ALS lines.

(A) Illustration of transcriptome profiling of HB9::GFP$^+$ versus PHOX2B::GFP$^+$. (B) Heatmap indicates differentially expressed genes between PHOX2B::GFP$^+$ and HB9::GFP$^+$ in *SOD1^{A4V}*(n=3 for each group, n means independent batches of differentiation; technical replicates) and *C9ORF72* ALS lines (n=3 for each group, n means independent batches of differentiation; technical replicates). (C-E) Dot plots represent Top 15 gene sets over-represented in HB9::GFP$^+$ compared to PHOX2B::GFP$^+$. Single ALS lines were analyzed in panel C and D for *SOD1^{A4V}* and *C9ORF72*, respectively. Those two lines were combined and analyzed together in panel E to validate the data. Individual dots are sized to reflect the number of genes in each gene set. (F) Illustration of transcriptome profiling

of HB9::GFP$^+$ versus PHOX2B::GFP$^+$ in hESC and hiPSC lines. (G) Heatmap indicates differentially expressed genes between PHOX2B::GFP$^+$ and HB9 antibody-stained cells in control (hESC+hiPSC) lines (at least n=4 for each group, n means independent batches of differentiation; technical replicates). (H) Dot plot shows commonly over-represented GO terms of HB9::GFP$^+$ cells compared to PHOX2B::GFP$^+$ cells in control (hESC+hiPSC) lines (at least n=4 for each group, n means independent batches of differentiation; technical replicates). (I) Heatmap indicates differentially expressed genes between combined PHOX2B::GFP$^+$ and HB9 antibody-stained cells in control (hESC+hiPSC) lines (at least n=4 for each group, n means independent batches of differentiation; technical replicates) and HB9::GFP$^+$ in ALS hiPSCs (*C9ORF72*+*SOD1*^{A4V}) (n=3 for each group, n means independent batches of differentiation; technical replicates). (J) Combined dataset of the two ALS lines show the same over-represented GO terms comparing to combined PHOX2B::GFP$^+$ and HB9 stained cells of control lines (hESC+hiPSC) (at least n=4 for each group n means independent batches of differentiation; technical replicates).

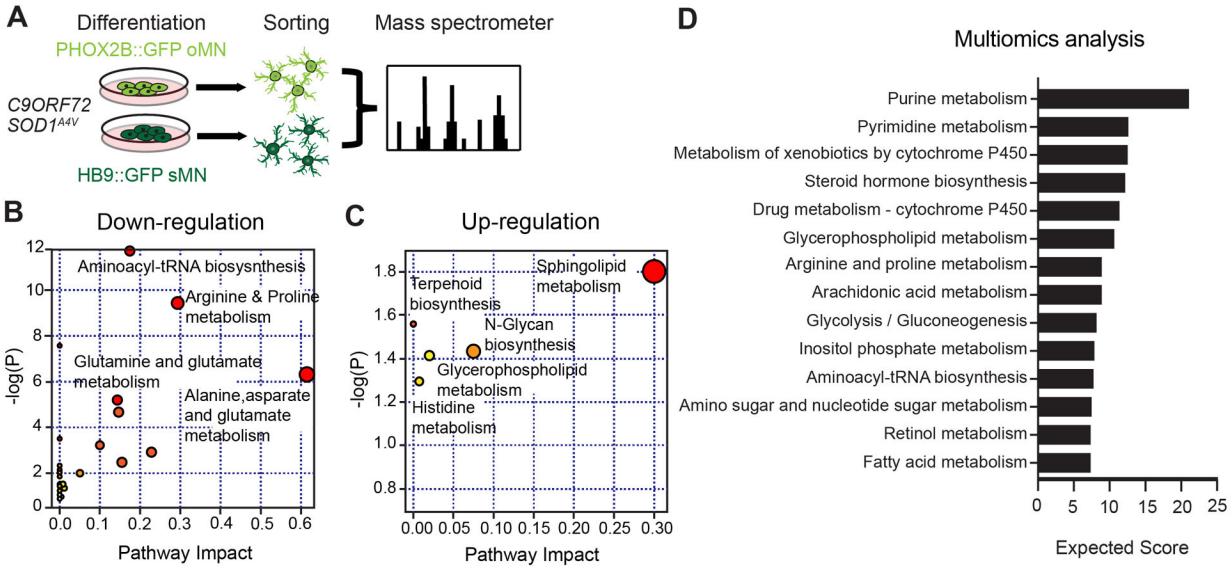

Fig. 3. Metabolomics analysis indicates up-regulation of lipid metabolism in post sorted HB9::GFP^{+} of *SOD1*^{A4V} and *C9ORF72* ALS lines.

(A) Schematic illustration of post-sorted metabolomics analysis. (B-C) Pathway analysis by MetaboAnalyst v.4.0 shows up-regulated and down-regulated metabolisms (n=3 for each group, n means independent batches of differentiation, each circle represents a different pathway; circle size and color shade are based on the pathway impact and p-value (red being the most significant), respectively (Detailed statistical analysis in Methods section). (D) Glycerophospholipid, fatty acid and arachidonic acid metabolism are highly enriched in expected score of multi-omics analysis (n=3 for each group, n means independent batches of differentiation; technical replicates).

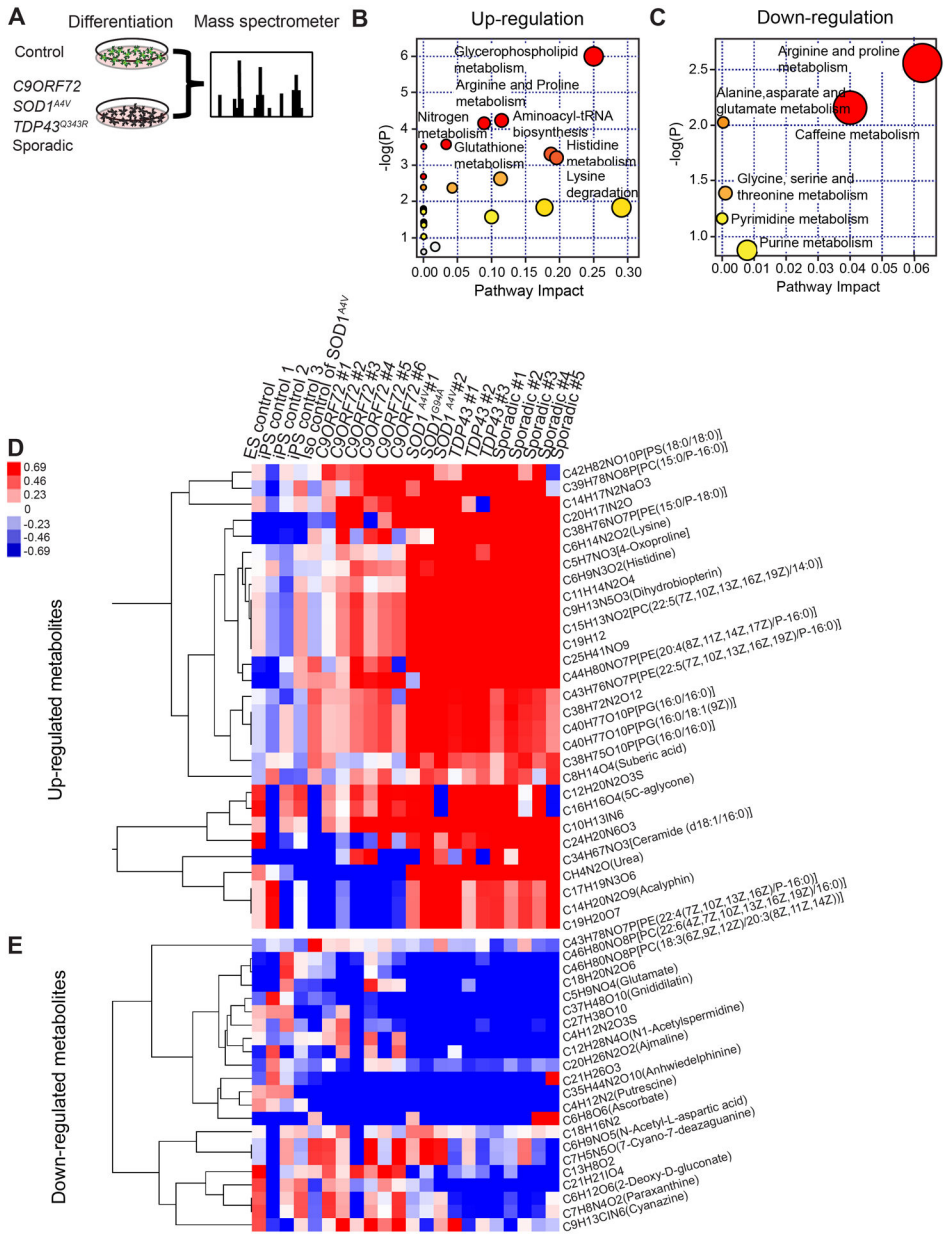

Fig. 4. Metabolomics analysis in un-sorted sMN differentiation confirmed up-regulation of lipid metabolism, and provides lipid related metabolic candidates in *TDP43^{Q343R}*, *C9ORF72*, *SOD1^{A4V}* and sporadic ALS lines.

(A) Schematic illustration of un-sorted metabolomics analysis. (B and C) Glycerophospholipid metabolism is highly up-regulated (B) in pathway analysis of unsorted *SOD1^{A4V}*, *C9ORF72*, *TDP43^{Q343R}* and sporadic sMN differentiation (each circle represents a different pathway; circle size and color shade are based on the pathway impact score and p-value (red being the most significant), respectively. Detailed statistical analysis in Methods section.). (D and E) Heatmap shows up-regulated and down-regulated metabolites candidates from unsorted multiple lines of ALS sMN differentiation (n=3 for each group; technical replicates, n means independent batches of differentiation; n=1 hESC healthy control, n=3 hiPSC healthy control, n=1 isogenic control hiPSC of *SOD1^{A4V}*, n=6

C9ORF72 ALS hiPSC lines, n=3 *SOD1* ALS hiPSC lines, n=3 *TDP43* ALS hiPSC lines, n=5 sporadic ALS hiPSC lines, n means independent hESC/hiPSC line number; biological replicates).

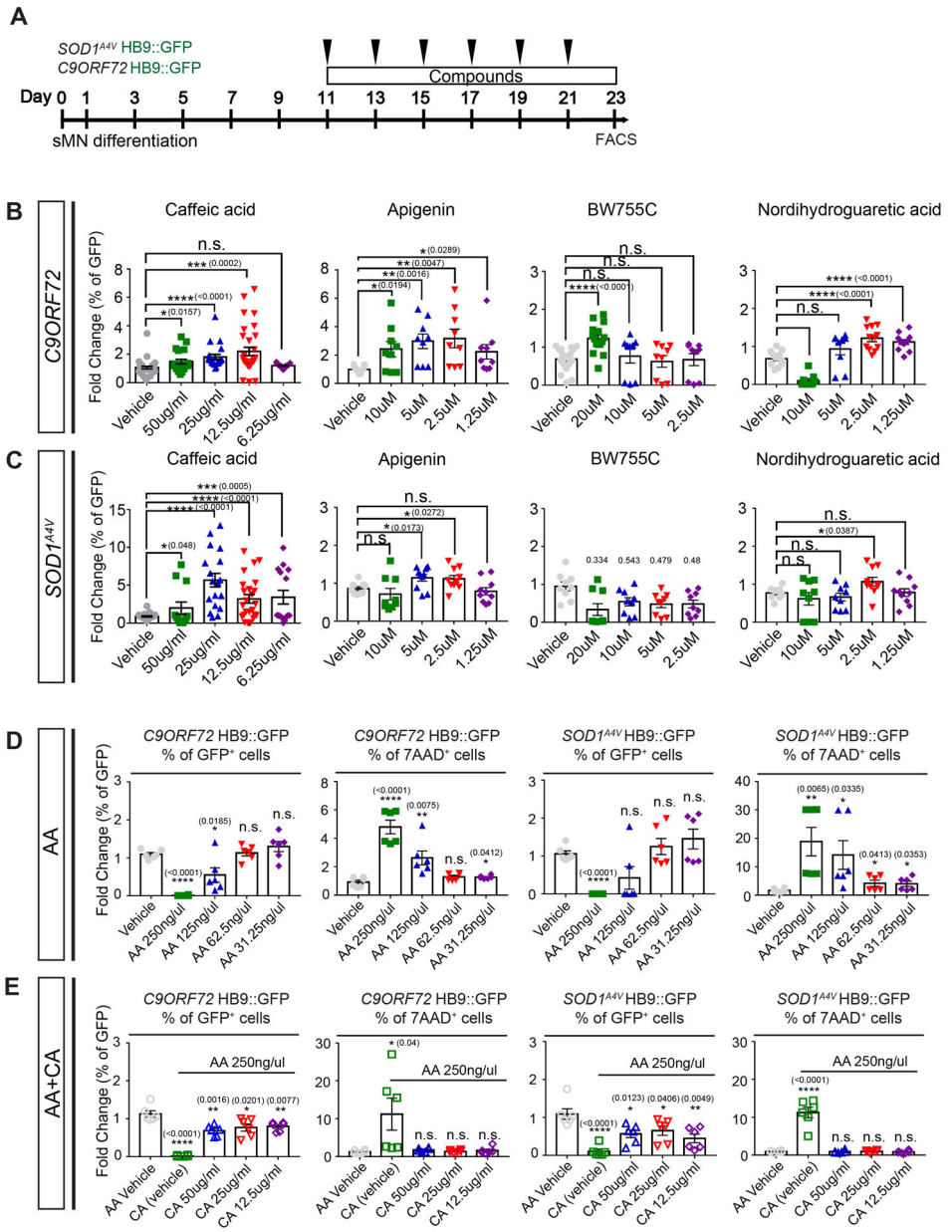

Fig. 5. 5-LOX inhibitors rescue motor neuron degeneration *in vitro*.

(A) Schematic timeline of compounds treatment during sMN differentiation. (B-C) Administration of 5-LOX inhibitors (Caffeic acid, Apigenin, BW755C and Nordihydroguaretic acid) in *C9ORF72* (B) and *SOD1*^{A4V} (Caffeic acid, Apigenin and Nordihydroguaretic acid) (C) sufficiently rescue the reduced levels of HB9::GFP^{+} cells (D11 – D23, *P<0.05, **P<0.01, ***P<0.001, ****P<0.0001, n.s.: not significant, two-tailed; unpaired student's t-test; each dot indicates individual wells from at least 3 experimental repeats/batches; p-values are indicated in each graph). (D-E) Treated AA in sMN culture reduced the percentages of HB9::GFP^{+} cells and induced the percentages of 7AAD^{+} cells of *SOD1*^{A4V} and *C9ORF72* by FACS analysis (D), but CA treatment reversed the levels of HB9::GFP^{+} cells and 7AAD^{+} cell (E) (complete media; n=6, each dot

indicates individual wells from 2 experimental repeats/batches; technical replicates; n.s.: not significant, *P<0.05, **P<0.01, ****P<0.0001, two-tailed; unpaired student's t-test; p-values are indicated in each graph). Error bars: mean ± SEM.

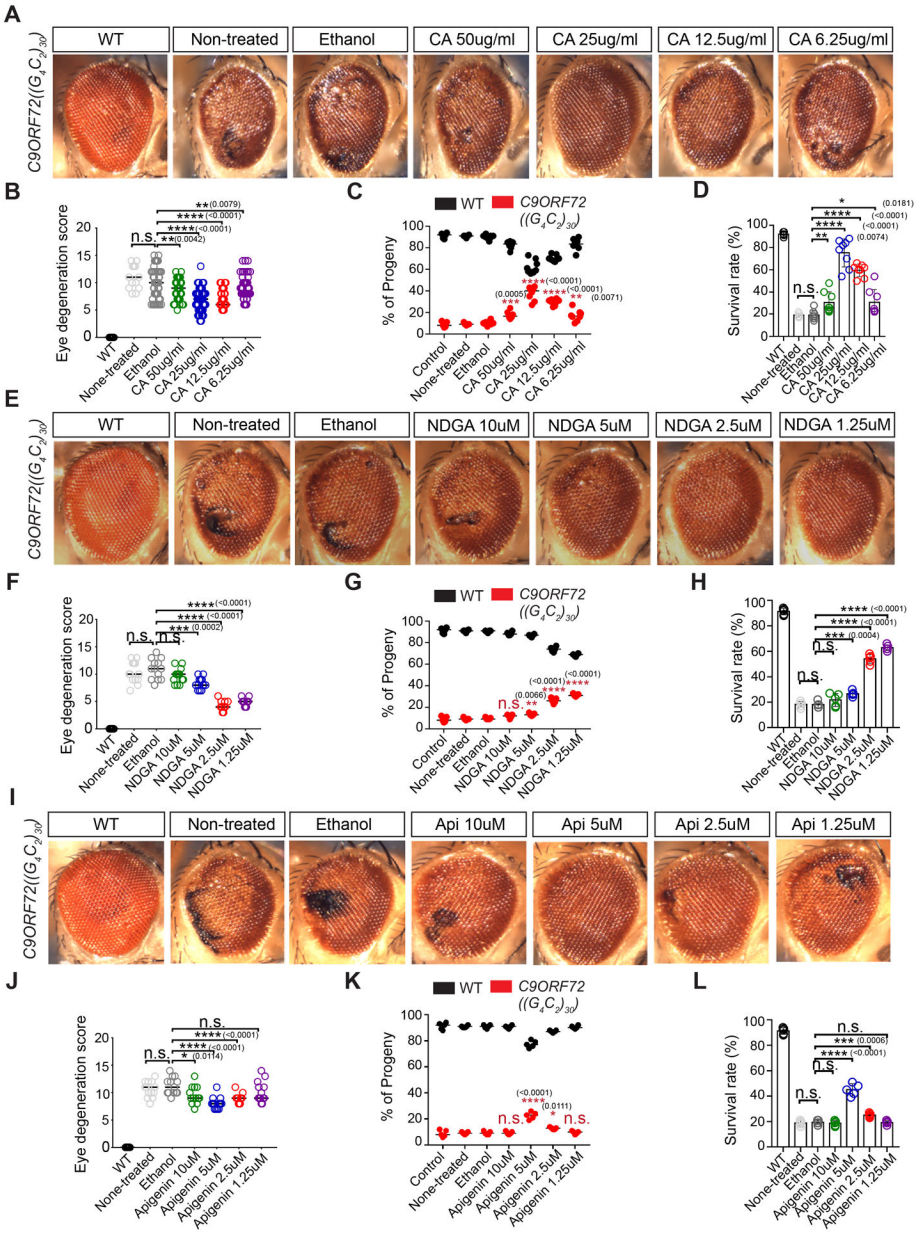

Fig. 6. 5-LOX inhibitors rescues the phenotype of *Drosophila* model.

(A-B, E-F, I-J) Dose dependent compounds rescue of eye degeneration in *C9ORF72(G4C2)30) Drosophila* model (CA (caffeic acid); 6.25 μl to 50 μl, NDGA (nordihydroguaiaretic acid); 1.25 μM to 5 μM, Api (apigenin); 2.5 μM to 5 μM; at least n=13 for each group; n.s.: not significant, *P<0.05, **P<0.01, ***P<0.001 ****P<0.0001, two-tailed; unpaired student's t-test; p-values are indicated in each graph). (C-D, G-H, K-L) Progeny efficiency and survival rate of *Drosophila* are also rescued by each compound feeding (n=5 for each group, n.s.; not significant, *P<0.05, **P<0.01, ***P<0.001 ****P<0.0001, two-tailed; unpaired student's t-test; the percentage of adult progenies (*C9ORF72* and WT progenies) from (♀w1118 × ♂OK371-Gal4; UAS-(G4C2)30/TM6B, GAL80 genetic cross); p-values are indicated in each graph). Error bars: mean ± SEM.

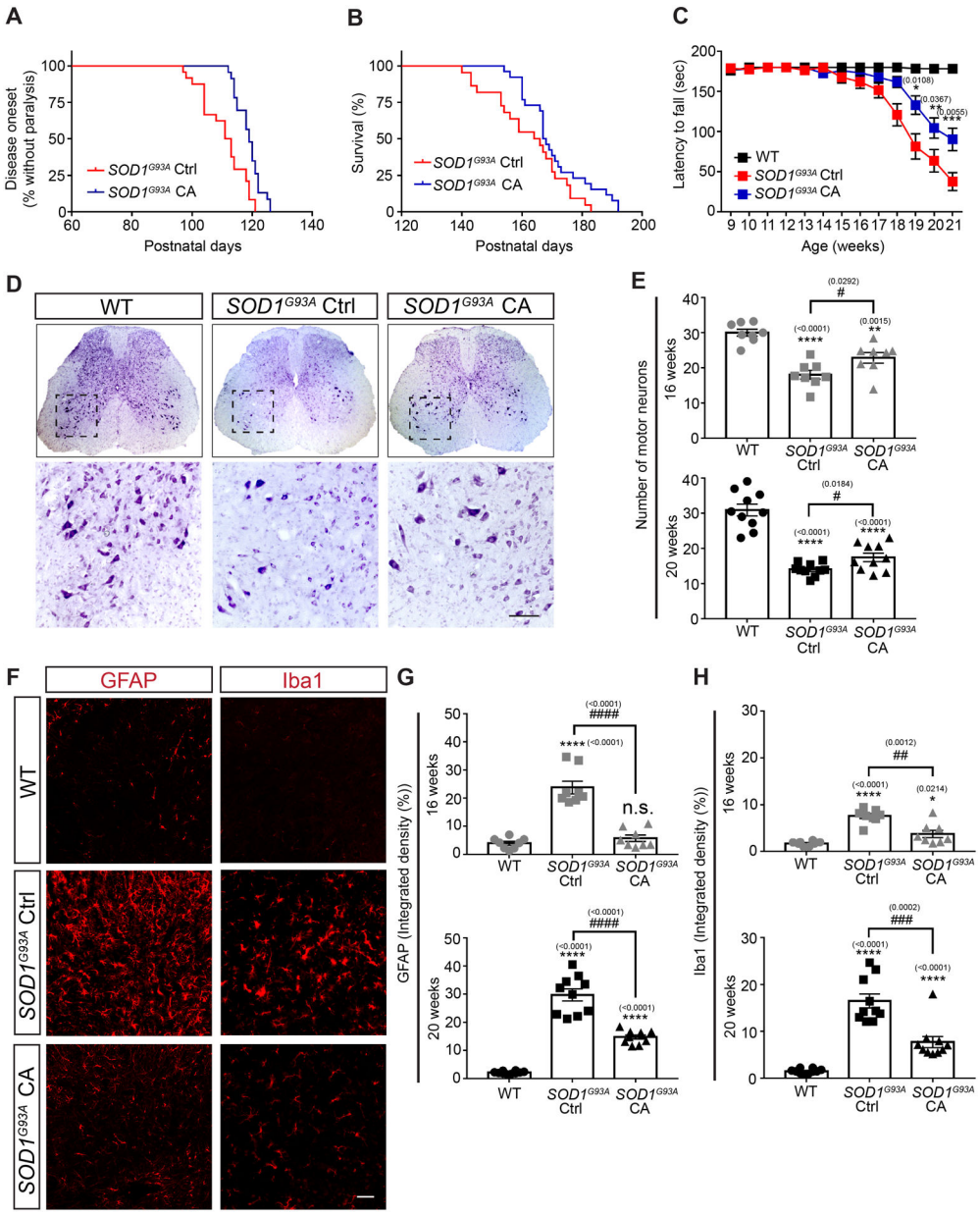

Fig. 7. Caffeic acid alleviates disease pathogenesis in *SOD1*^{G93A} mice.

(A-B) Kaplan-Meier curves of disease onset (A) and mice survival (B) in *SOD1*^{G93A} mice. (C) Locomotor performance evaluated by the rotarod test (n=24 for each group). (D) Cresyl violet staining (Nissl staining) to visualize the motor neuron in L4-L5 segments of the spinal cord at early symptomatic stage (16wks) (n=10 for each group) (Scale bar: 100 μm). (E) The number of motor neuron in L4-L5 segments of the spinal cord (n=8 for each group at 16 weeks; and n=10 for each group at 20 weeks). (F) Activated astrocytes (GFAP) and microglia (Iba1) in L4-L5 segments of the spinal cord at early symptomatic stage (16wks) (Scale bar: 50 μm). (G) The integrated density of fraction area stained with GFAP at the indicated time points (n=8 for each group at 16 weeks; and n=10 for each group at 20 weeks). (H) The integrated density of fraction area stained with Iba1. (n=8 for each group

at 16 weeks; and n=10 for each group at 20 weeks) (WT: wild-type mice; Ctrl: vehicle administered *SOD1*^{G93A} mice; CA: caffeic acid (30 mg/kg) administered *SOD1*^{G93A} mice; *,#, $p < 0.05$; **,##, $p < 0.01$;***,###, $p < 0.001$ and ****,####, $p<0.0001$, n.s.: not significant, two-tailed; unpaired student's t-test; p-values are indicated in each graph). Error bars: mean ± SEM.